Christian Marco Pichler, BSc

Studies towards the synthesis of nanostructured nickel phosphide and tungsten carbide materials

MASTERARBEIT

zur Erlangung des akademischen Grades
Diplom-Ingenieur
Masterstudium Technische Chemie

eingereicht an der

Technischen Universität Graz

Betreuer
Prof. Dr. Rolf Breinbauer
Institut für Organische Chemie der TU Graz

Prof. Dr. Ferdi Schüth
Max-Planck-Institut für Kohlenforschung, Mülheim a.d. Ruhr

Graz, August 2014

Die vorliegende Arbeit wurde unter Leitung von Prof. Dr. Ferdi Schüth in der Zeit von Februar bis Juli 2014 in der Arbeitsgruppe für heterogene Katalyse und funktionale Feststoffe am Max-Planck-Institut für Kohlenforschung in Mülheim a.d. Ruhr angefertigt.

“I am still confused, but now on a higher level.”

Enrico Fermi

Acknowledgements

I would like to thank first and foremost *Professor Dr. Ferdi Schüth* for giving me the great opportunity to carry out my master thesis in his group on such a fascinating topic. I am very grateful for the guidance, motivation and freedom he granted me during my work. I also appreciate the chance of gaining new knowledge and skills through his seminars and talks.

Furthermore I would like to express my gratitude to *Professor Dr. Rolf Breinbauer* for encouraging me to conduct this work in Mülheim. I also want to thank him for his support during my entire stay in Germany and his interest in my topic.

I am also very much obliged to *Dr. Guanghui Wang* for his support, advice and the assistance with TEM measurements. I also appreciate the interesting and fruitful discussions and his companionship very much.

Additionally I want to thank:

Dr. Wolfgang Schmidt, for guiding me in the work with the analytical instruments and for the support with the SAXS measurements.

Flora Godor, Nicolas Duyckaerts and *Jacob Abildstrøm* for proofreading individual chapters.

Andre Pommerin and *Tobias Zimmermann* for the assistance in building up experimental setups.

Bernd Spliethoff, Hans Bongard and *Ann-Christin Swertz* from the TEM department such as *Dr. Claudia Weidenthaler* from the XRD department for various measurements and supportive data evaluation.

Finally I also want to thank my office mates *Daniel Wendt, Jacob Abildstrøm, Dr. Gonzalo Prieto, Dr. Felix Richter* and all the other members of the group for the friendly welcome in the group, the numerous activities inside and outside of the institute and making my stay very special and pleasant.

Abstract

The present work investigated and compared different synthesis pathways for creating nanostructured nickel phosphide and tungsten carbide materials. To fulfill this task, adequate support materials were chosen. For supporting the nickel phosphide, hollow polymer shells, containing free carboxylic acid groups, were used. Under high temperature and reductive conditions the hollow polymer shells formed hollow carbon shells that retained the previous structure. Several deposition techniques for nickel phosphide were applied to create small and dispersed Ni_2P particles. It emerged that the direct phosphidation method yielded the material and the Ni_2P particles with the best characteristics. In this method the free carboxylic acid groups were crucial to ensure a good distribution of the nickel particles. The direct phosphidation pathway consisted of two steps: 1.) the deposition of metallic nickel particles on the hollow polymer shells followed by carbonization, 2.) the direct phosphidation of these nickel particles to Ni_2P with trioctylphosphane as phosphorous delivering agent.

For the tungsten carbide materials a different support was used, namely a nitrogen-doped, ball-shaped polymer support with porous texture, which could also be carbonized, whereby its structure was retained. Herein the nitrogen was responsible for enabling a decent distribution of the carbide particles. The carbidization could be observed at high temperatures (800 °C) and under reductive atmosphere, whereas the carbon for the carbide formation was delivered from the support material itself. Nevertheless, the carbide particles were well dispersed and had a size of 3-5 nm. In further experiments it was tried to lower the reaction temperature by adding transition metals, which could facilitate the carbidization process. These experiments confirmed that there are two different carbidization mechanisms for inert and reductive conditions, respectively. Under inert conditions preferably WC was formed, whereas under reductive atmosphere W_2C was the major phase. Finally it was shown that transition metals, like nickel, could facilitate the carbide formation under both reaction conditions.

Table of Contents

1. Introduction

One of the greatest challenges in our days for global society is the shift of our fossil fuel based energy system to renewable energy sources. There are many reasons to promote this shift, and one of the major ones is the challenge of global warming. The anthropogenic CO_2 emission, caused by burning of fossil fuels, is considered to make a major contribution to this phenomenon.[1] Also the depletion of fossil resources has to be faced.[2] Even if it is complex to estimate how long there will be a sufficient supply of these resources, there will be a point when the extraction of petroleum is not feasible at reasonable prices any more. From the European perspective also the economic point of view shall not be underestimated. Germany, for example, has to import 68 % of its primary energy sources.[3] Therefore the usage of local renewable resources possesses also an economic benefit.

Especially in Europe great efforts have already been made to increase the energy production by wind and solar power.[3][4] Also for the individual transportation sector alternative technologies are developed and brought to market, such as fuel cell or battery-driven cars. This is in contrast to heavy transportation vehicles (ships, trucks, airplanes) where the change from liquid hydrocarbons as fuel to other options seems to be very unlikely, considering the alternatives developed so far. Therefore the production of liquid hydrocarbon fuels from renewable sources was and is heavily promoted. This resulted in the fast growth of biodiesel production from fats and oils or bio-ethanol production from sugar or starch containing crops, which are both already used today as blending agent for fossil derived fuels.[5] However, there is one major drawback of the biofuels produced today. The plants that are most widely used for its production such as corn, sugar cane, oil containing crops and many more could also be used for food and fodder supply. The usage of great quantities of plants for conventional biofuel production causes competition with aliment production, which cannot be justified facing growing earth population and recurrent famines in developing countries. This dilemma requires the use of biomass that does not compete with aliment production. Hence the conversion of lignocellulosic biomass to liquid hydrocarbon fuels is a very appealing goal. Lignocellulosic biomass is very abundant and includes agricultural residues (straw, sugarcane bagasse, corn stover), forest products (wood, saw dust) and dedicated crops (switchgrass, salix).[6] This means that for these feedstocks there exists no competition with food production – although there is still some competition with respect to land use.

Lignocellulose is a very stable compound, consisting of cellulose, hemicellulose and lignin making the separation of the single compounds and conversion into biofuel challenging.[7] There are two approaches how to convert lignocellulose into processable materials. The first one is to separate the cellulose and hemicellulose from the lignin. Usually harsh reaction conditions are necessary to achieve this, like in pulp and paper milling. The alternative is to directly convert the biomass (wood, straw etc.) by pyrolysis under high temperature and

pressure into a liquid substance called biooil. The biooil cannot be used directly as transportation fuel, because it contains a very high amount of oxygen (approx. 40 %).[8] This makes storage difficult due to the lack of chemical stability. Thus, the oxygen content has to be lowered by deoxygenation reactions.[9] A possible method to do this is via a catalyzed reaction with hydrogen by performing a hydrodeoxygenation (HDO), which is the analogous process to hydrodesulfurization (HDS) a crucial step in refining petroleum to fuel. A biooil based hydrocarbon mixture with lowered oxygen content (<4 %) would serve as an excellent transportation fuel.[9] Like for many hydrogenation reactions platinum group metals are good catalysts, which is also valid for hydrodeoxygenation reactions. However, platinum group metals are a limited resource and therefore very expensive. Taking the emerging propagation of fuel cell technology into account, which also needs platinum as catalyst, the demand for these metals is likely to rise. Thus the finding of a catalyst that can perform the HDO-reaction without platinum group metals is a highly relevant task.

Possible candidates to fulfill this assignment are transition metal phosphides and carbides. It was discovered by M. Boudart already in the 1970's that these materials have similar electronic structures like platinum group metals and consequently similar reactivity in catalytic reactions.[10] This necessitates the deeper investigation and further development of these catalytic materials. Especially Ni_2P and W_2C are very interesting compounds with promising catalytic properties.[11][12] The finding or improving of synthesis methods for these compounds should therefore be pursued and would promote the possibility of biofuel production from lignocellulosic biomass.

2. State of the art

2.1 Lignocellulose as biofuel feedstock

Concerning the European plan on climate change, which was launched in 2007, the goal of the European commission is to reach a share of 10 % of biofuels in the total consumption of vehicles in 2020.[13] Similar goals can be found in the USA where the target for 2030 is to produce 20 % of transportation fuel and 25 % of chemicals from biomass.[9] Especially the conversion of lignocellulose to liquid hydrocarbons as transportation fuel is a desirable goal due to the fact that the production of lignocellulosic biomass does not compete with aliment production. Additionally, lignocellulose is abundant and can be grown faster with lower costs compared to biomass feedstocks used today (corn, oil containing plants etc.).

Lignocellulose consists of cellulose, hemicellulose and lignin which makes the separation of the single compounds and conversion into biofuel challenging. The general structure of lignocellulose is depicted in Figure 2.1.

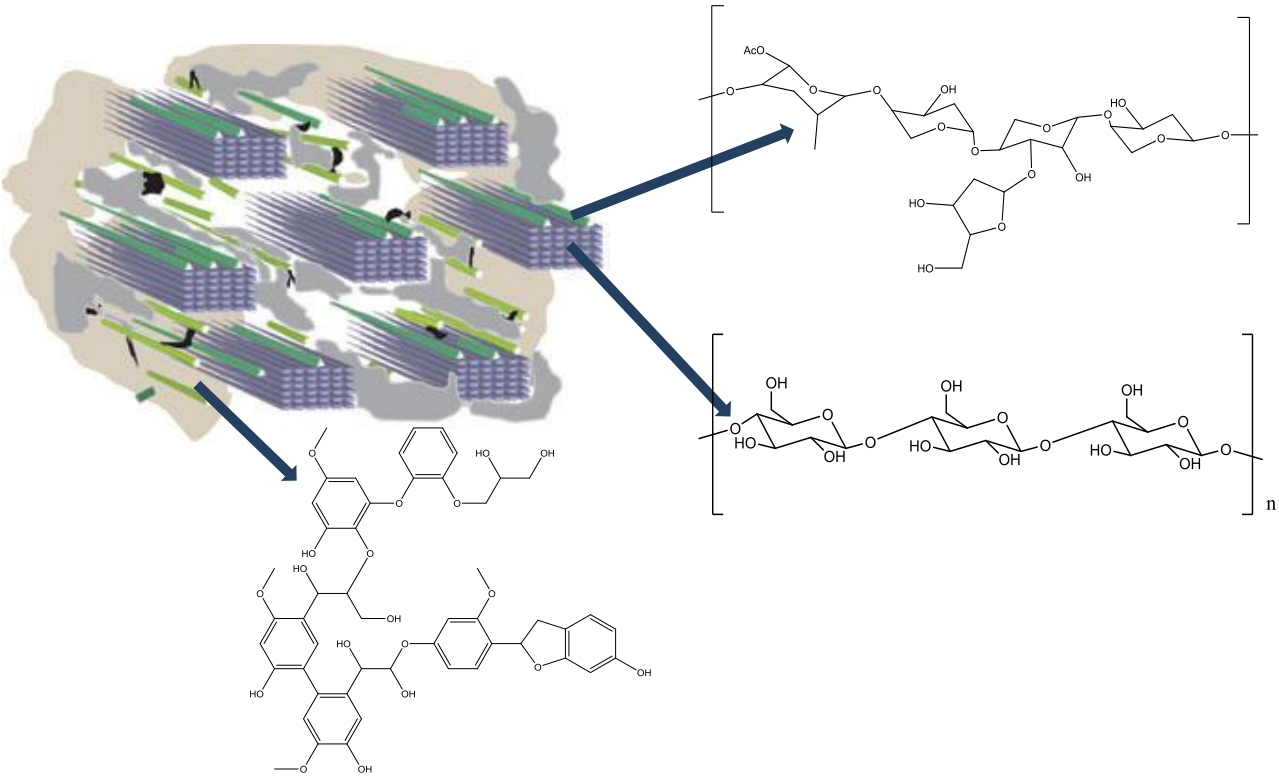

Figure 2.1 Schematic structure of lignocellulose and chemical structures of cellulose, hemicellulose and lignin (Picture taken from Ref. [14]*)*

The blue elements show the rigid cellulose fibers which are macromolecular chains of 1,4-β-glycosidic linked glucose molecules. The green rods depict the hemicellulose that is also formed by polymeric chains containing different sugars such as xylose, mannose, arabinose and also glucose. The matrix in which all these components are embedded is lignin, drawn as the gray background in the picture. Lignin possesses a complex structure based on

aromatic molecules that are crosslinked by ether formation between the aromatic motifs. The tight coherence of these elements explains the difficulties for separation of the single compounds. Separation of single components of the lignocellulose is one of several processing possibilities that are illustrated in Figure 2.2.

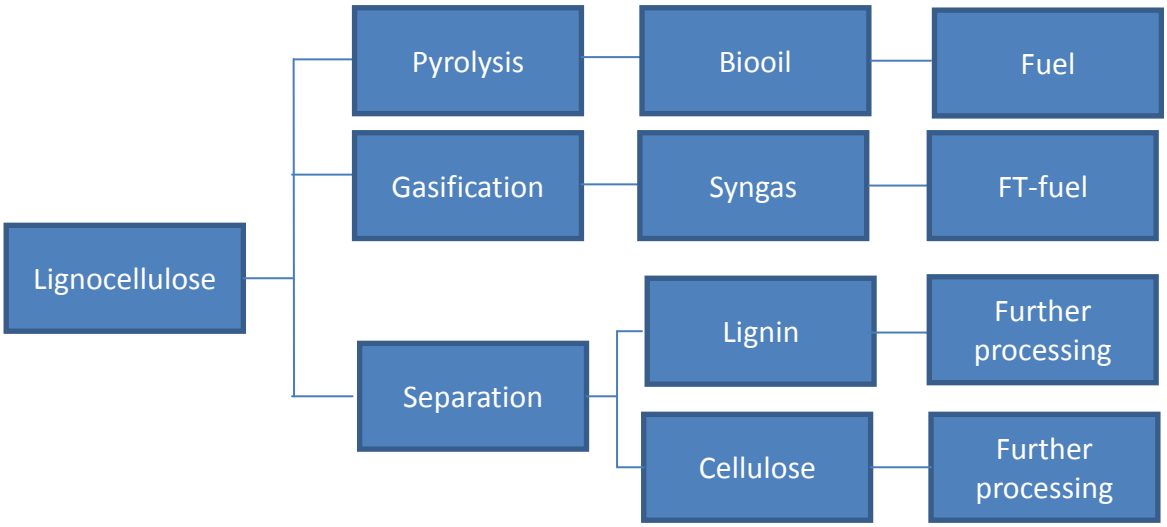

Figure 2.2 Lignocellulose processing [8]

Typically the cellulose is required to be separated from the lignin, before any further processing. To accomplish this, usually harsh conditions are necessary, like in pulp and paper processing where high temperatures around 180 °C and severe chemical treatment by strong bases (NaOH) or acids (H_2SO_4) are used.

Recently more gentle methods have been developed to overcome these drawbacks. This is for example a ball milling process which is capable of converting wood directly into a water soluble sugar fraction and a solid lignin fraction. This process ensures a high yield and subsequently a separate processing of the sugar fraction and the lignin.[15]

However, when the production of fuel is the primary goal, a direct use of the whole lignocellulose without previous separation would be favorable. One possibility for this task is the biomass-to-liquid-process, which combines two well-known processes: the biomass gasification and the Fischer-Tropsch (hereby denoted as F-T) synthesis.[16] The gasification takes places at high temperatures of about 800 - 1100 °C under oxidizing atmosphere (air, oxygen).[17] For fuel production it is desirable to obtain as much syngas as possible meaning that CO and H_2 shall be the main products. To adjust the right ratio of these two components also the watergas shift reaction can be applied, where CO is converted with H_2O to yield CO_2 and H_2. Other parameters also play an important role, when it comes to the production of the optimal gas mixture, like the reactor design, particle size and shape of lignocellulose material, residence time and the oxidizing atmosphere, which all have to be optimized for gasification. The resulting syngas can then be used for Fischer-Tropsch synthesis of hydrocarbons.

2.2 Bio-oil production

Besides the gasification route there exists also another method to convert lignocellulosic biomass into a transportation fuel. The lignocellulose can be subjected to pyrolysis at 400 - 600 °C under inert atmosphere.[18] Under these conditions the chemical bonds in the lignocellulose can be cleaved and the macromolecules of cellulose and lignin are decomposed to smaller units. The resulting products are a solid char, gaseous compounds, and a liquid fraction called bio-oil that contains more than 400 different single compounds, like aldehydes, ketones, acids, esters, aromatic compounds, and other residues derived from lignin and cellulose.[19] The listing of the compound types indicates that bio-oil possesses a very high oxygen content of about 40 % additional to a water content of about 25 %, which must be taken into account for further processing.[20][21] Also in the pyrolysis process there are many parameters that can be varied to adapt the procedure for a high yield of bio-oil. To fulfill this task mostly fast pyrolysis is used, where the biomass is exposed to temperatures of about 450 °C with a residence time of 1 s in a fluid bed reactor. The functioning of these reactors is well understood and with the right pretreatment of the biomass (water content 10% and particle size <3 mm) a yield of 70-75 % of bio-oil (related to dry biomass) can be achieved.[18]

Besides the already mentioned characteristics of bio-oil, like the high oxygen and water content, also the acidity of about pH 2.5 is notable.[18] Considering all these facts together, it is evident why bio-oil cannot be used directly as a transportation fuel. The low pH value of bio-oil would cause severe corrosion in an ordinary internal combustion engine. In addition, the blending with regular gasoline or diesel is not possible because bio-oil is not miscible with these fuels. Furthermore, the storage stability of bio-oil is not granted as all the oxygen containing functional groups, like aldehydes, ketones and others, are reactive and change the properties of the stored bio-oil when reacting with each other. Additional problems are the lower heating values compared to conventional gasoline (16-19 MJ/kg vs. 46 MJ/kg) and the high viscosity which can cause difficulties when pumping and transferring the liquid.[22] In spite of all these challenges the production of fuel derived from bio-oil there are also advantages compared to F-T fuel. The process set-up for the pyrolysis of biomass is simpler compared to biomass-to-liquid-process because it requires only a single reactor. It can also have a smaller throughput (of ca. 50-100 tons per day) which is beneficial for decentralized and local fuel production.[22][23] Such small plants would be economically unviable for F-T plants. However, to promote the use of bio-oil derived from pyrolysis some requirements have to be fulfilled:

- Chemical stability must be increased
- Heating value shall be increased
- Viscosity must be decreased
- Better miscibility with conventional fuels has to be achieved

All these requirements could be met, if the oxygen content could be decreased. The typical threshold of oxygen in a final fuel would be below 4 %, but in a first step also oxygen contents between 5-10 % would be acceptable, because this would enable the miscibility with conventional gasoline fuels.[9] This implies that the oxygen is bound as low acidity alcohols (meaning no phenolic groups or acids). Compared with the content of other elements such as sulfur (10-50 ppm) or nitrogen, an oxygen content of 4 % is still a comparatively high value. However, a further reduction of oxygen is not required because E10 and E20 fuels (gasoline blended with 10 % respectively 20 % of ethanol) are already commercially available and do not cause problems by having an oxygen content of 3.5 % and 7 % respectively. Quite the contrary, it seems that a certain level of oxygen will even improve the burning characteristics of fuels by decreasing soot formation.[24]

2.3 Deoxygenation strategies

The removal of certain elements, like sulfur or nitrogen, from oil is a crucial step in the refining of petroleum to fuel. A lot of effort has been made to develop desulfurization processes and the associated catalysts for petroleum. This development permitted the production of ultra-low-sulfur diesel fuel with a sulfur content of <10 ppm to meet the Euro V standards. In contrast, processes for deoxygenation of oils were not very intensively researched. This is due to the fact that there is typically only a low amount of oxygen present in petroleum, and so the need for deoxygenation has not arisen before. The situation changed when alternative fuel production was launched and the production of relevant amounts of bio-oil became possible. This increased the research interest in suitable catalysts for deoxygenation reactions.

2.3.1 Deoxygenation without additional hydrogen

The first possibility for deoxygenation is cracking with zeolites, which is just an adaption of this widely used technique from conventional petroleum refineries. In petroleum refining, high boiling heavy oils are converted into lower boiling fractions by cracking. Regarding the bio-oil, the deoxygenation is an additional task. The goal is to obtain products with higher chemical and thermal stability and lower oxygen content. Typical reaction conditions are 700 °C under air with a zeolite catalyst such as ZSM-5 or zeolite Y in an FCC (fluid catalytic cracking) reactor. The scheme of such a reactor is shown in Figure 2.3.[25] It can be seen in this picture how the catalyst circulates in the tubes together with the educts. The coke formed in this process is then burned in the regenerator which also delivers heat for this process at the same time.

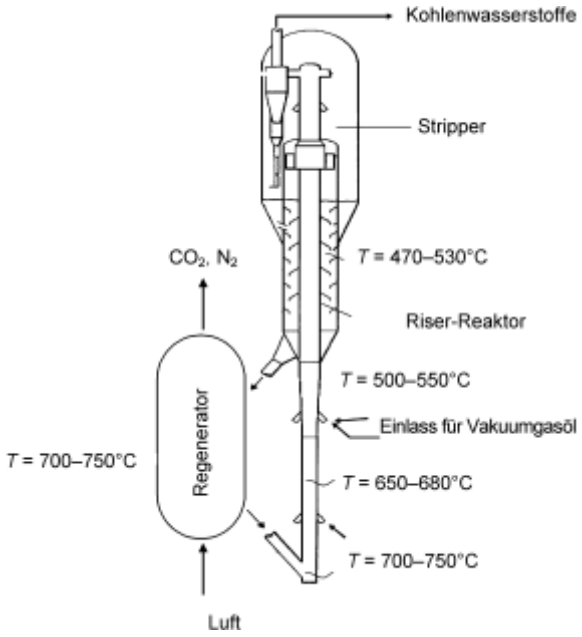

Figure 2.3: FCC reactor (Picture taken from Ref. [25])

The main reaction products are aliphatic and aromatic hydrocarbons, but also gases (especially CO and CO_2) and water are formed in great amounts. A multiplicity of different reactions will take place during this reaction and the most important ones are listed in the following:

- Dehydration: Especially alcohol groups can be eliminated as water molecule and leave an olefin behind. Also intramolecular dehydrations of e.g. two vicinal OH-groups are possible, yielding water and a ketone.

- Cracking: Long hydrocarbon molecules are split into smaller ones. Fragmentary molecules like propane and other gases are formed

- Hydrogen forming reactions: Different possibilities exist, how hydrogen can be formed. One of them is the watergas shift reaction. CO and H_2O are produced by other reactions and can then be converted to H_2 and CO_2.

- Hydrogen consuming reactions: All kinds of hydrogenation are likely to happen under these conditions. The common ones are hydrogenations of ketones or aldehydes to alcohols but also olefins can easily be converted to alkanes.

- Decarboxylation/Decarbonylation: Carboxylic acids and aldehydes can eliminate CO_2 respectively CO under these temperatures. These reactions are crucial for lowering of the total oxygen content of the bio-oil and reduce the chain length of the hydrocarbons.

- C-C bond forming reactions: All kinds of condensation reactions are also taking place under these conditions, such as ether or ester formation and Claisen-condensation. Very prominent is also the aldol-condensation. These reactions play also an important role for lowering the oxygen content.

- Coking: In some tests the formation of coke was up to 30 % relating to the used bio-oil, which shows the importance of this reaction. Mainly aromatic species, like phenols, guajacols and others, are accounted for coke formation. These stable aromatic motifs are also found in the coking products. The connection of the single aromatic molecules is often enabled by dehydration reactions between these molecules. To prevent this, some authors suggested that these coke forming molecules shall be extracted with water before the cracking process.[25][26]

It can be seen from the above mentioned reactions that the basic steps of the whole cracking process are hydrogen donation and consumption reactions. Hydrogen is produced and consumed directly during the different reactions. It is also evident that a higher amount of in situ generated hydrogen can facilitate the deoxygenation. This is the reason why sometimes the naphtha fraction from conventional petroleum refineries is added to bio-oil to serve as hydrogen donor.[27]

The advantages of this process are the advanced engineering and reactor technology, due to the long chain of development of this process in conventional petroleum industry. The same holds for the zeolite catalysts which are also thoroughly investigated. On the other hand the FC-cracking also has disadvantages, like the extensive coke formation. Even if the coke can be burned for generation of process heat, the yield of liquid hydrocarbon product is reduced by coke formation.[25] Also the suggestion to diminish coke formation by extraction of aromatic compounds prior to the reaction contains drawbacks. Aromatic hydrocarbons are important compounds for the quality of fuel and they are especially added to gasoline for performance improvement. The fact that bio-oil is already containing aromatic species should be exploited and not require an additional extraction step. Eventually a final oxygen content of <4 % shall be reached. To achieve this goal while still obtaining hydrocarbon chains with an appropriate length for the use as fuel is a very demanding challenge for this system. All these are reasons for the development of alternative deoxygenation processes.

2.3.2 Hydrodeoxygenation

The roots of hydrodeoxygenation (HDO) are also located in the petroleum refineries. It was nitrogen and especially sulfur that should be removed during the refining. This was done to minimize the sulfuric oxide emissions during burning of the fuel in vehicles and to prevent the poisoning of the car catalyst, amongst others. High pressures of hydrogen and adequate catalysts are used to convert the sulfur into volatile H_2S which can then be removed and further processed. The same principle is used for HDO reactions were additional hydrogen is

used to convert the bound oxygen from the bio-oil into H_2O. Compared with FCC the hydrodeoxygenation has higher costs due to the need of extra hydrogen.[25] However, the development of new more selective catalysts and the expectation of cheaper hydrogen production by the shift of electric energy production to renewable resources – although this view is not unequivocally shared - makes the HDO a very interesting alternative that should be closely investigated.

2.4 Transition metal sulfides (TMS)

Due to the fact that HDO has many similarities with the hydrodesulfurization (HDS) reaction, it is obvious to test the well characterized and investigated HDS catalysts also for their HDO activity. For this reason a remarkable number of publications can be found in the literature that deals with the investigation of TMS catalysts for HDO reaction.[28] The most common catalysts for industrial HDS reaction are MoS_2 catalysts that are either doped with cobalt or nickel. The corresponding catalysts are denoted as Co-MoS_2 and Ni-MoS_2.[9] The doping of the sandwich-like MoS_2 crystal structure with cobalt enhances the catalytic activity of the material as the cobalt prefers to occupy edge positions in the lattice where it weakens the molybdenum-sulfur bond and induces vacancies. These generated vacancies can then serve as active sites in hydrodeoxygenation.[28] Other authors suggest that the cobalt atom itself can also function as an active site.[29]

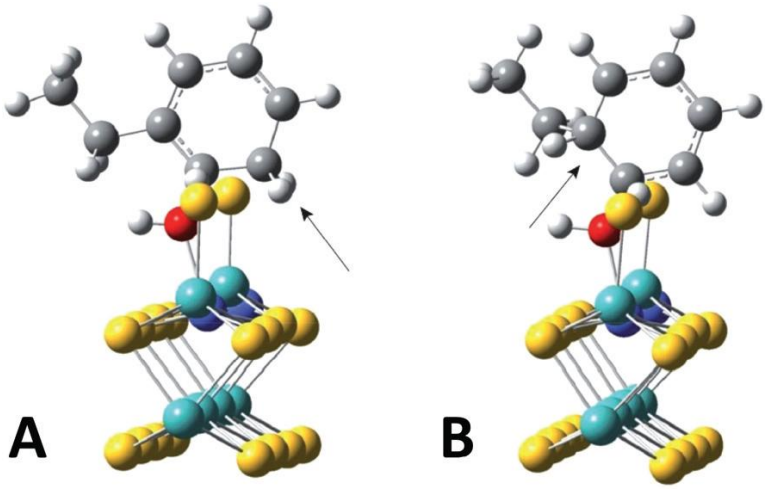

Figure 2.4: Co-MoS_2 structure (yellow=sulfur, light blue=molybdenum, dark blue=cobalt, red=oxygen, grey=carbon, white=hydrogen) (Picture taken from Ref. [30])

Figure 2.4 shows the structure of a Co-MoS_2 with an adsorbed oxygen containing species. The adsorption of the oxygen on the active site is also the first step in deoxygenation reactions, which can follow two different pathways on TMS catalysts. The first pathway is the direct deoxygenation (DDO). It starts with an adsorption of the molecule's oxygen atom on a vacancy. This is followed by a donation of an H-atom from the ubiquitous S-H groups (resulting from the dissociative adsorption of H_2 molecules) to the attached molecule by

forming a carbocation. Then the C-O bond is cleaved while the oxygen is released as water forming the deoxygenated compound.[28]

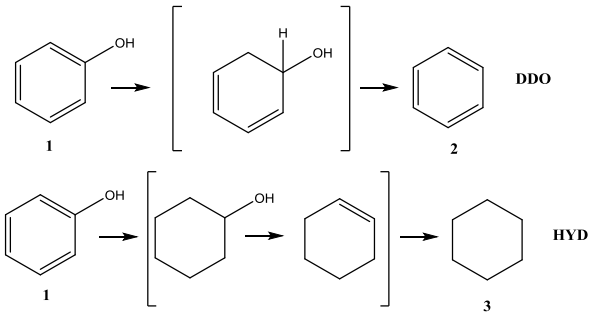

Figure 2.5: DDO and HDO mechanism [9]

In the second mechanism, called hydrogenation (HYD) mechanism, all unsaturated carbon-carbon bonds are first hydrogenated followed by the deoxygenation. The particular share of the single reaction mechanism depends on several factors which are summarized in Table 2.1.

Table: 2.1 Comparison between typical HYD and DDO conditions [9]

HYD-mechanism	**DDO-mechanism**
Ni doped MoS_2 catalysts	Co doped MoS_2 catalysts
Lower temperatures	Higher temperatures
Presence of inhibiting molecules (NH_3…)	No inhibiting molecules

Like every catalyst, also the transition metal sulfides can be deactivated during the reaction. Besides the conventional deactivation mechanisms, such as loss of surface area, aggregation of catalyst particles, and coke formation (which is promoted by polyoxygenated aromatics), a special aspect has to be considered with these catalysts. This is the oxidation of the sulfides to oxides. The sulfur can be continuously removed during reaction conditions for example by formation of H_2S or different species. At the same time it will be replaced by oxygen, forming metal oxides. Some promoters can slow down this process, but they cannot prevent it completely.[31] To ensure the stability of the sulfide catalyst additional sulfur compounds, mainly H_2S, have to be added to the feed stream. The H_2S will then react again with the formed oxides and will restore the sulfide catalyst. According to literature, several thousand ppm of H_2S are added to a feed stream.[32] This is a major disadvantage of this catalyst type, because the addition of sulfur compounds to the feed stream will result in an elevated sulfur content of the resulting product. This raises the question if the fuel produced with these catalysts can meet the strict requirements regarding sulfur content. The latest EU and US laws demand ultra-low-sulfur fuel where the sulfur content may not exceed 10 or 50 ppm. Also the economical aspect of providing an additional H_2S stream should not be underestimated and may affect the feasibility of the whole process.

Even though the TMS catalysts show a certain activity for the HDO reaction, the problem with the addition of H_2S to the feed stream remains, which poses challenges regarding the resulting fuel quality but also economical and technical questions.

2.5 Noble metals

An alternative would be the use of noble metals, or specifically platinum group metals, to catalyze this reaction. They are very good hydrogenation catalysts and are also industrially used for these reactions. Therefore they have been extensively studied. Another advantage over the TMS catalysts is that there is no additional H_2S feed necessary, and platinum group metals are not as susceptible to deactivation by water compared to the sulfides.[9] Especially the latter reason is very important for reaction with bio-oils, as they contain a high amount of water. The platinum group metals possess many advantages and are therefore good candidates for the HDO reaction of bio-oils.

The general deoxygenation mechanisms are similar to the sulfide catalysts. At first there is again a competition between the DDO and the HYD mechanism as depicted in Figure 2.6. Besides the fully deoxygenated products, also compounds containing oxygen can be found. Figure 2.6 depicts some of the possible products that can be formed from guajacol during HDO reactions.

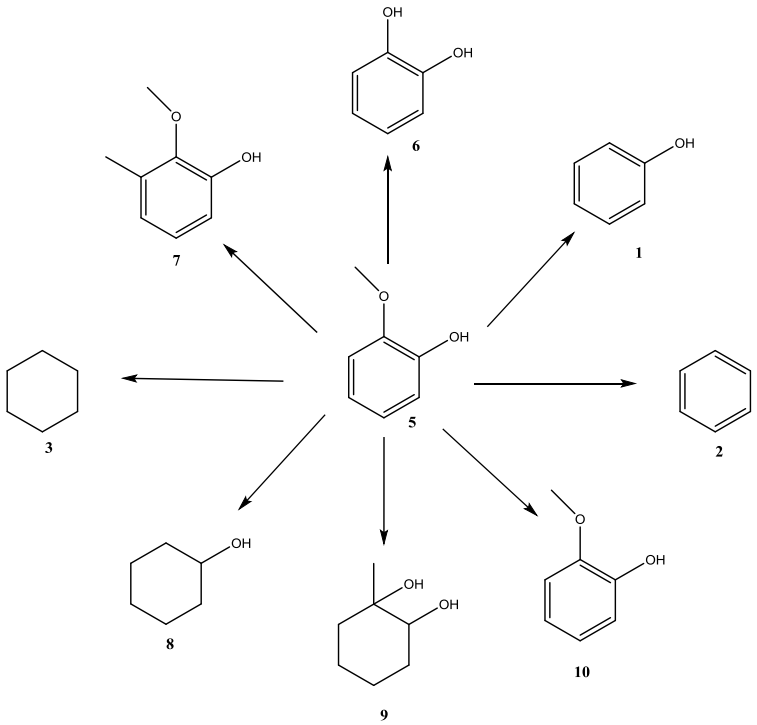

Figure 2.6: Reaction products of guajacol [33][34]

The diversity of the different products shows that beside DDO and HYD also other reaction mechanisms can occur. Very common are, amongst others, demethylation and

methyltransfer reactions leading to products **6**, **7** and **9**. The precise product distribution depends on many factors, including reaction conditions like temperature and pressure, but also the catalyst properties, such as catalyst composition, support material and particle size. In the following part some of these influences are discussed, taking the reaction of guajacol as an example.[33][34]

Temperature:

At low temperatures (100 °C) the hydrogenation of the aromatic ring is favored compared to deoxygenation reactions. The main products found at this temperature are cyclohexanol, cyclohexanone and other saturated compounds. Raising the temperature to 300 °C the deoxygenation of guajacol is dominating and products like benzene, toluene and others are formed.[33] The reason for this is the change of Gibbs free enthalpies ΔG of the products with temperature as shown in Figure 2.7. At low temperatures the formation of saturated compounds is thermodynamically favored, which changes with increasing temperature.

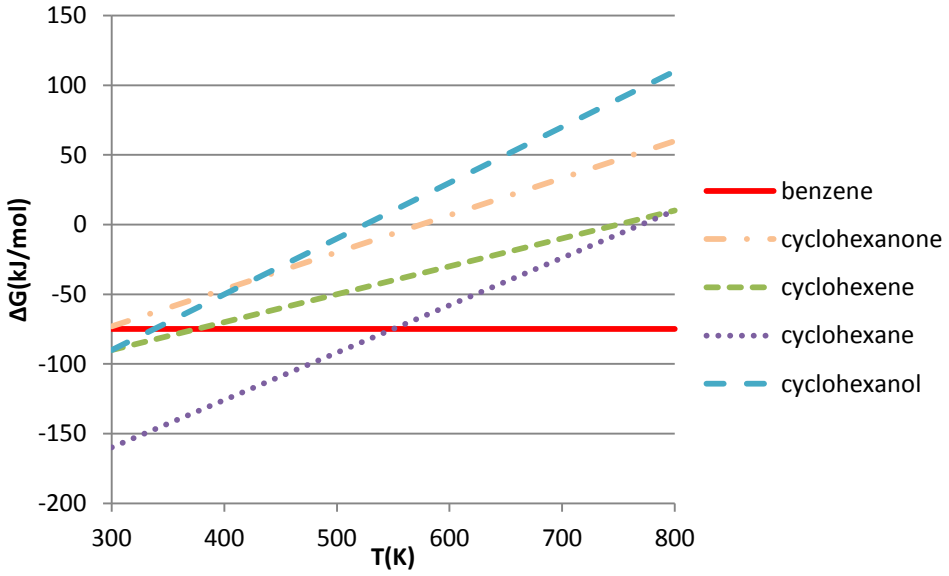

Figure 2.7: Gibbs energies of HDO products as function of temperature (Picture taken from Ref. [35])

Catalyst and support properties:

The use of different noble metals results in different conversions and product distributions. A study by Varma et al.[36] compares the reaction of guajacol with different noble metals supported on carbon. The results are shown in Figure 2.8 and the different activity and product distribution of the single metals can be clearly seen.

Catalyst	Conversion after 200 min
Pt/C	88%
Pd/C	70%
Rh/C	57%
Ru/C	50%

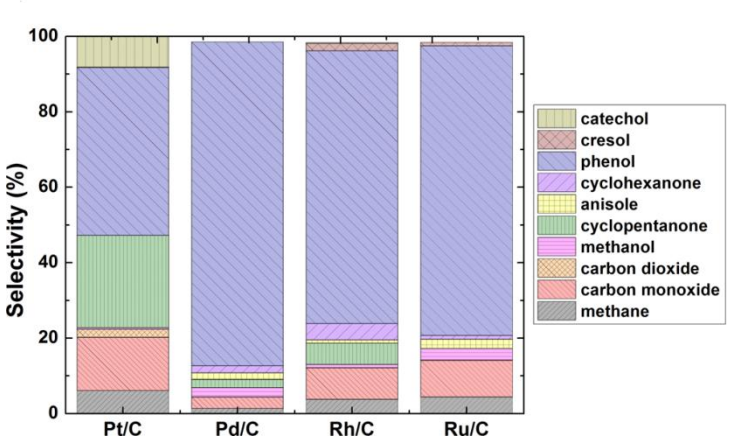

Figure 2.8: Different reactivity of noble metals (Picture taken from Ref. [36])

By mixing the noble metals with each other or doping with different metals like cobalt or nickel the selectivity and reactivity of the catalyst can be further tuned. Also the interaction with the support must not be underestimated. Frederick et al.[35] compared the reaction of phenol on ruthenium catalysts on different supports and found also varying activities and product distributions. The yield of deoxygenated products varied between 25% for Ru/Al_2O_3 and 86% for Ru/TiO_2. The reason for the higher activity of the TiO_2 support is a spillover mechanism, where dissociated hydrogen atoms on the Ru reduce a Ti^{4+} to a Ti^{3+} center. This Ti^{3+} center enables the adsorption of the phenolic oxygen, which then facilitates the deoxygenation of the phenol. Another observed phenomenon was: when the Ru particles grow larger, the amount of saturated product is increased. In this case the phenol adsorbs preferentially with its aromatic ring on the metal particle and not with its oxygen on the Ti center. The adsorption via the aromatic ring then facilitates its hydrogenation. This should be kept in mind for the design of future catalysts.

The deactivation of the noble metal catalysts is caused by particle growth, loss of support surface area and especially coking which is promoted by the aromatic species found in bio-oil. The acidity of the support is important for coke formation and it is assumed that high surface acidity enhances coke formation.[33][37] Thus the catalyst support has to be selected carefully.

As it was previously shown, noble metals have certain advantages for the HDO reaction. They show a good activity for the reaction, they are well studied, and the product selectivity can be even altered by changing metal or support. Nevertheless they also possess major drawbacks namely their high price and limited availability. Emerging renewable technologies like fuel cells also require these metals, implying an even rising demand. Hence the finding of an alternative catalyst that has similar reactivity but contains more abundant metals would be preferable.

2.6 Transition metal phosphides and carbides

Exchanging the high priced noble metals with more abundant materials that show a similar activity is not a new idea. Already in 1973 Levy and Boudart found that tungsten carbide shows a platinum-like catalytic behavior and is active in isomerization reactions that are typically catalyzed by platinum.[38] This discovery raised the interest in other metal/non-metal compounds and it turned out that transition metal phosphides and nitrides show similar catalytic properties.[39] These materials were then tested for their catalytic behavior in several reactions, which were typically conducted with noble metal catalysts. Especially the use of transition metal phosphides and carbides for the HDS and HDN reactions was studied. Amongst others, Oyama and co-workers proved the activity of phosphides and carbides for these reactions in their studies.[40][41] The interest to use transition metal phosphides and carbides also for the HDO reaction has increased only over the last 5-10 years, when the necessity for the upgrading of bio-oil at a bigger scale appeared. As these materials show promising catalytic activity, both properties and synthesis methods have to be explored and investigated.

Several reasons are discussed, why these compounds have a different catalytic activity compared to the corresponding metal catalysts. One reason is that the incorporation of the non-metal atoms causes a ligand effect. Electron density is shifted between the metal and the non-metal and this generates a change in band energies and electronic structures. Furthermore the lattice dimensions change through the incorporation of the non-metals. The next factor is the so called ensemble effect. This effect prevents the formation of bulk oxides, which is usually a common deactivation mechanism. Since the metal atoms are not direct neighbors anymore and less of them are exposed to the catalyst surface, the bulk oxide formation is hindered. Finally also the non-metal is not simply a spectator, but can also take part in the catalytic mechanism, which influences the resulting activity.[9]

2.6.1 Properties and synthesis methods of tungsten carbide

The special catalytic properties of this material class were firstly discovered in tungsten carbide, and it is still today one of the materials with the most promising properties and catalytic activities. Tungsten carbide forms different phases, depending on synthesis temperature and carbon content. The phase diagram in Figure 2.9 shows all these different phases derived from the two compounds WC and W_2C. Two phases are the most observed under usual synthesis conditions: There is the fcc β-WC phase that shows a NaCl analogue crystal structure, meaning the carbon atoms occupy all octahedral voids of the fcc-lattice formed by the tungsten atoms. The second one is the W_2C phase, where the tungsten atoms form a hexagonal sublattice and half of the trigonal prism interstitials are occupied by carbon atoms.[9]

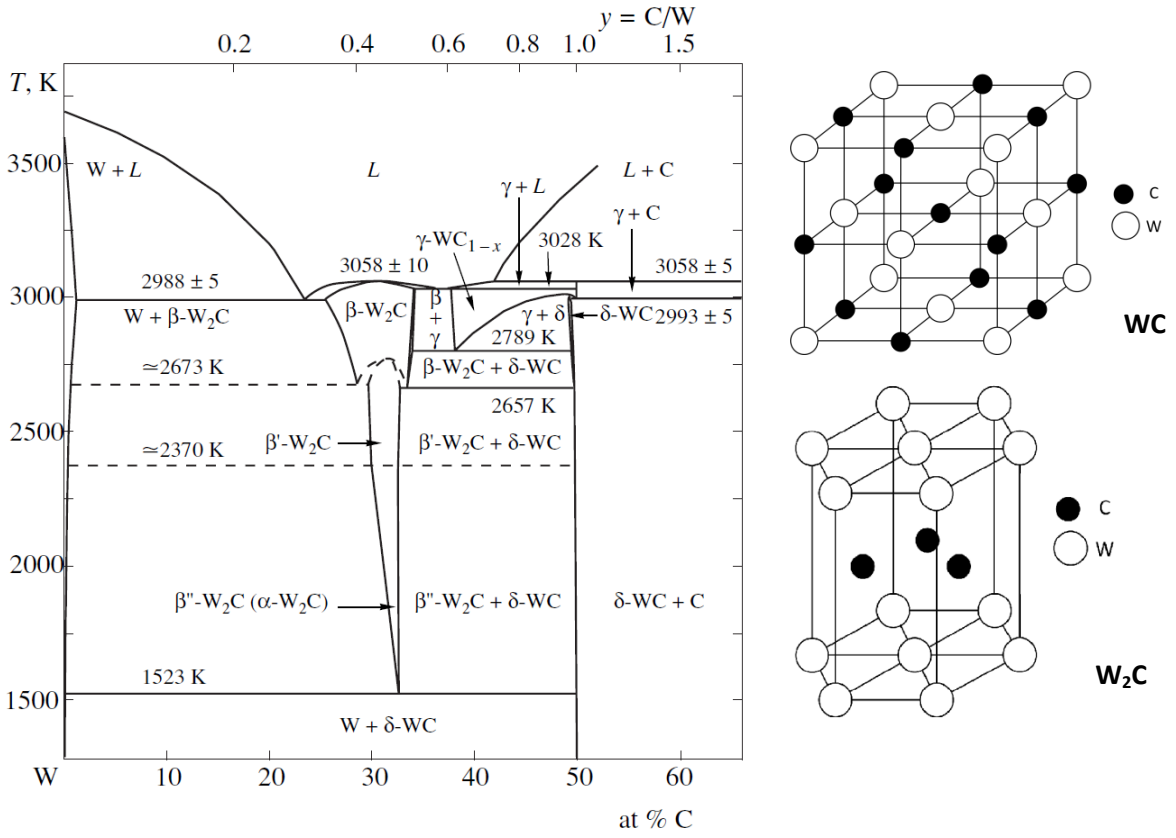

Figure 2.9: Phase diagram and crystal structures of WC (pictures taken from Ref. [9][42]*)*

In the metallurgical industry tungsten carbide is often produced by solid phase reaction between the tungsten metal or oxide with a carbon source (mostly graphite) at high temperatures of around 900-1200 °C. This is not common for catalyst synthesis. Herein gas phase carbidization is the most widely used technique. A tungsten oxide precursor (pure or dispersed on a substrate) is reacted at temperatures between 700-900 °C with a mixture of hydrogen and a carbon containing gas like methane or ethane. The tungsten oxide will be reduced stepwise and converted to the carbide. The stoichiometry of the following reactions was not considered and the reaction equations were adopted unmodified from reference. [43]

$$WO_3 + H_2 \longrightarrow WO_{3-x} \quad (1)$$

$$WO_{3-x} + H_2 \longrightarrow WO_2 + H_2O \quad (2)$$

$$WO_{3-x} + H_2 + CH_4 \longrightarrow WC_xO_y + H_2O + CO_2 + CO \quad (3)$$

$$WC_xO_y + CH_4 \longrightarrow W_2C + H_2O + CO_2 + CO + H_2 \quad (4)$$

$$W_2C + CH_4 \longrightarrow 2\,WC + 2\,H_2 \quad (5)$$

The sequence of the reaction proceeds with higher temperature. Reaction (1) starts around 550 °C whereas the W_2C phase is formed at around 600 °C and the WC phase will appear at around 750 °C. This only holds for conditions with 10 % CH_4 in H_2 and with pure bulk WO_3 as starting material. If the WO_3 is supported the reaction temperature and the sequence may change due to support interactions or hindered accessibility of the WO_3 particles. The gas

phase carbidization exhibits the disadvantage that carbon can be deposited onto the solid substrate. Therefore also another synthesis method for the carbides was developed, namely the carbothermal reduction method. This method can only be used when the carbides shall be produced on a carbon support. If this is the case, no additional carbon containing gas is required. Firstly a tungsten oxide precursor is dispersed on a carbon support. After heating the solid up to around 700-800 °C under hydrogen atmosphere, the formation of tungsten carbide is observed.[44] The oxide precursor will undergo reduction reactions comparably to reactions (1) and (2). The carbon donor for the carbide formation is in this case the support itself. Carbon can diffuse into the tungsten lattice and occupy the interstitials and thereby the carbides are formed. With the mentioned synthesis method also other transition metal carbides can be formed, for example the molybdenum carbide.

Compared with other catalysts there are only few studies that investigate HDO reactions with carbide catalysts (especially tungsten carbide). One study by Bitter et al.[45] investigates the activity of carbon supported tungsten carbide for the deoxygenation of fatty acids. This study could prove that the carbide shows good selectivity for the HDO reaction compared to the decarboxylation reaction, where CO_2 would be lost through the reaction. The latter reaction pathway is favored by tungsten oxide. This difference is explained through the platinum-like character of the tungsten carbide, which is capable of chemisorbing hydrogen at its surface and therefore promoting the HDO reaction.

The same group released also a study where carbon supported W_2C and Mo_2C catalysts were used for the HDO reaction of guajacol.[46] The Mo_2C catalyst showed a better conversion than the W_2C catalyst (99% vs. 81%), but the product distribution was similar for both catalysts. The main products were phenols and cresols. Fully deoxygenated products like benzene or toluene only made up 5% of the products in the best cases. Saturated products such as cyclohexane or cyclohexanol were only detected in small amounts around 2-7%. The most promising factor of about these carbide catalysts is their overall high activity in guajacol conversion. Nevertheless, there is also a drawback which is the low yield of fully deoxygenated products. In contrast, the low selectivity for saturated products is again an advantage. Unfortunately, there are very few studies that investigate the reaction mechanism of the HDO reaction on carbide catalysts. The studies conducted so far suggest that the substrate adsorbs via its oxygen containing functional group on the surface. Then the chemisorbed hydrogen on the surface can attack the oxygen atom and promote the HDO reaction.[45] That means that besides the adsorption of the substrate also the chemisorption of hydrogen is a crucial step in the reaction. Another study by Chen et al.[47] examines the adsorption of furfural on Mo_2C surfaces. It is suggested that the main interaction of the furfural adsorption is caused by the aldehyde group of the furfural. This is another indication that the interaction of oxygen containing functional groups with the carbide surface is preferred.

There are not many studies investigating systematically the deactivation mechanisms of the metal carbides. The existing information suggests that the main deactivation mechanisms are also for these catalysts particle aggregation, loss of surface area and coke deposition. An important issue that has to be considered is the chemical stability of the carbides under reaction conditions. A possible deactivating reaction is the oxidation of the tungsten carbide by oxygen containing species in the feedstock or water yielding WO_2 or WO_3. Whether bulk oxides or only surface oxides are formed, is still an open question. Also the oxidation of the exposed surface carbon atoms resulting in C-O surface species is one possible reaction. In theory the reductive decomposition of the carbides could also be possible (considering the high H_2 concentration), yielding metallic tungsten and methane. However, this reaction is endothermic and was so far only investigated in theoretical studies.[9]

2.6.2 Properties and synthesis methods of nickel phosphide

Also metal phosphides and especially nickel phosphide show promising results for HDO reactions. Similar to tungsten carbide also nickel phosphide form several different phases dependent on phosphorus content and temperature, as the phase diagram in Figure 2.10 illustrates.

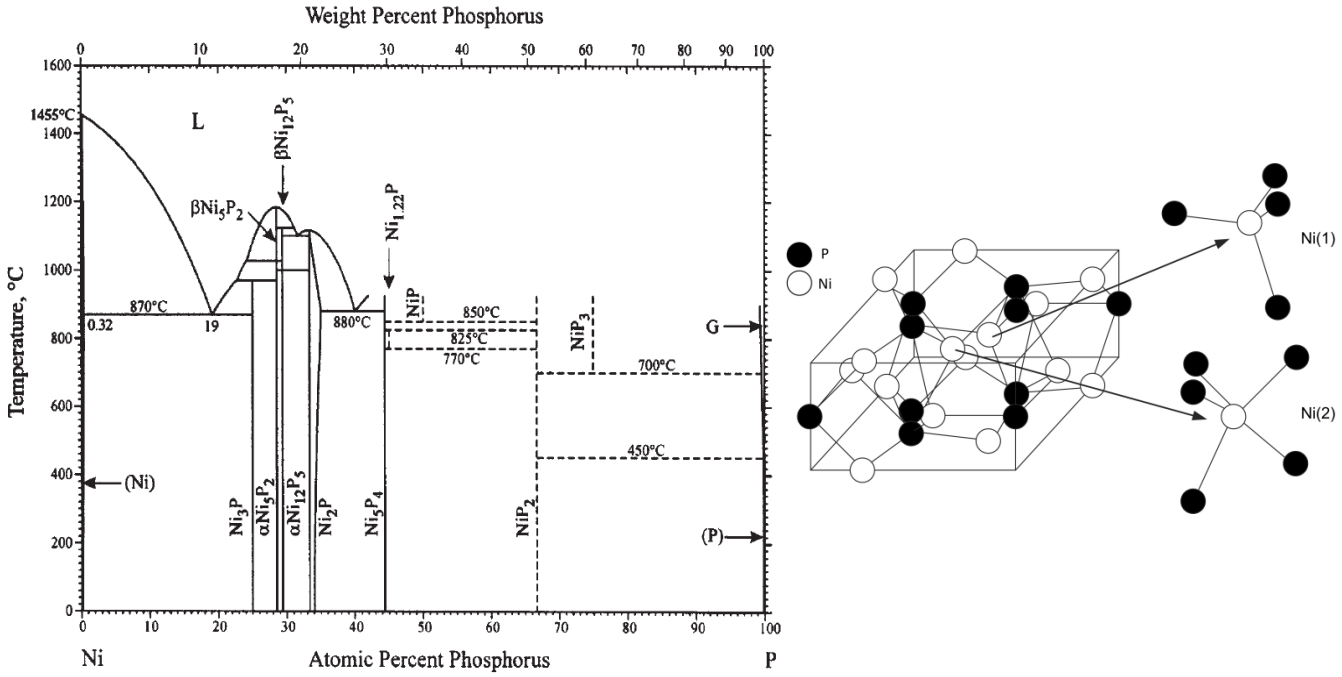

Figure 2.10: Ni-P phase diagram and Ni_2P crystal structure (Pictures taken from Ref. [41][48])

What distinguishes the phosphides is the fact that they are not interstitial compounds like the metal carbides. Phosphorus has an atomic radius of 0,109 nm, thus it is larger compared to carbon which has a radius of only 0,065 nm. Therefore phosphorus does not fit into the interstitial sites of the metal lattice, and different crystal structures are formed, where the metal atoms form triangular prisms surrounding the phosphorus.[12] The most important phase for catalysis is the Ni_2P phase which has been shown to be the most active phase for

HDO reactions. It can be synthesized by choosing the right Ni/P ratio. The temperature is not that critical, because the high temperatures where Ni_2P decomposes are normally not reached during an ordinary synthesis protocol. The crystal structure of Ni_2P is depicted in Figure 2.11. The Ni_2P phase has a hexagonal crystal structure and contains two different Ni centers. The Ni(1) center has a tetrahedral coordination, whereas a pyramidal coordination is found for the Ni(2) center. A striking fact is that the two nickel centers possess a different reactivity. In a study by Serrano et al.[49] the deoxygenation of methyloleate was examined it was found that the tetrahedral Ni(1) center was primarily active for decarboxylation reactions. In contrast the pyramidal Ni(2) center was very active for the HDO reaction. Oyama et al.[41] also encountered this phenomenon, when they investigated the HDS reaction of dibenzothiophene. They found that the Ni(1) atom carries out a direct desulfurization reaction whereas the Ni(2) center is active in a HYD mechanism. Additionally it was found that Ni(2) were rather located at the crystal surface.

There are different methods to synthesize Ni_2P: either as bulk compound or dispersed on support materials. The latter method is more important for catalyst production. A widely used method to synthesize supported Ni_2P is impregnation of the support with a precursor and subsequent reduction at elevated temperatures with hydrogen. Different precursors can be used:

- Phosphate reduction: A phosphate precursor can be prepared by impregnating a mixture of $Ni(NO_3)_2$ and $NH_4(H_2PO_4)$ on a support material followed by calcination at around 300 °C. Then the calcined material is reduced with hydrogen and the Ni_2P phase formation can be observed at around 600-650 °C. This method is comparatively facile and controllable. The disadvantage is the high temperature treatment which decreases the surface area of the final catalyst.[11]

- Hypophosphite reduction: A nickel salt (chloride, nitrate) is mixed with $NH_4(H_2PO_2)$ and the solution is impregnated on a support. So nickelhypophosphite is deposited on the support. This compound is not as stable compared to the phosphate and can thus be easier reduced. So with this method a reduction with hydrogen at 300-500 °C, depending on time and support, is necessary.[50]

- Phosphite reduction: Similar to the previous method a $Ni(H_2PO_3)_2$ precursor is impregnated on a support and then reduced with hydrogen at temperatures of approx. 500 °C.[51]

- Phosphane reduction: Instead of having the phosphorus already in the impregnation solution it can be also introduced by an external source, for example phosphane. In this case only metallic nickel or nickel oxide is supported and then reacted at elevated temperatures (400-500 °C) with a gaseous mixture of PH_3 and H_2 which will convert

the nickel or nickel oxide to Ni_2P. But also other phosphorus carriers can be used like trioctylphosphane (TOP), which is a liquid. By using TOP it can be avoided to use the highly poisonous PH_3, although the reaction has to be carried out in liquid phase.[52]

Despite the different synthesis methods the Ni_2P formation mechanism is very similar for all reactions. At first the nickel precursor is reduced to metallic nickel. The metal facilitates the H_2 chemisorption and the hydrogen is then available to reduce the phosphorus compound. The in situ reduced phosphorus can then diffuse into the Ni lattice and form the Ni_2P. Because of the necessary diffusion of the phosphorus, the elevated temperatures are very important. In the liquid phase methods, where TOP but no hydrogen is used, the TOP is just decomposed at the nickel surface and releases in situ the phosphorus.[53] The mentioned synthesis methods can be also used for production of other transition metal phosphides (MoP, CoP, RuP).

The next important task is the investigation of the activity for HDO reaction. Several authors compared the catalytic activity of different metal phosphides, and it was often claimed that nickel phosphide is more active than the analogous phosphides of Co, Fe, Mo and W.[40][54]

Wu et al.[55] studied the effects of different support materials for the HDO reaction of guajacol over Ni_2P catalysts. A change of product selectivity and overall conversion could be observed (Table 2.2). Likewise different Ni_2P morphologies were found on the single substrates. Bigger Ni_2P particles were observed on the Al_2O_3 support. The explanation for this fact is the very high reduction temperature of 900 °C that was necessary to observe formation of the phosphide, because the alumina interacts very strongly with the nickel precursor.

Table 2.2: Guajacol conversion over different Ni_2P catalysts (WHSV: 1.33 h^{-1}; T: 300 °C)[55]

Compound	**Ni_2P/SiO_2**	**Ni_2P/ZrO_2**	**Ni_2P/Al_2O_3**
Total conversion	99%	97%	99%
benzene	72%	26%	13%
phenol	2%	32%	31%
$CH_4/CO_2/CO$	6%	0%	6%
coke	11%	24%	40%

The higher coke formation for Al_2O_3 and ZrO_2 was explained through the interaction of guajacol with the Lewis acidic Al^{3+} respectively Zr^{4+} centers. In SiO_2 the authors claimed the guajacol would preferably interact with the Si-OH groups. This is a weaker interaction and so the coke formation is lower.

Other studies by Oyama et al. [56] investigated the deoxygenation of dibenzofuran. It was shown that Ni_2P catalysts were active in this reaction and the main product was dicyclohexane. Obviously here the formation of the saturated reaction products was again favored.

The comparability between different reaction studies is difficult, because each author uses different reaction parameters such as H_2 pressure or temperature. Also substrate, catalyst preparation and reactor setup (f.e. batch vs. flow setup) are varied. As the number of publications about the HDO reaction with Ni_2P catalysts is still comparatively low it needs more detailed and comparable studies to predict more general trends and draw valid conclusions. Some characteristic data of the studies that investigated the HDO-reaction on Ni_2P catalysts can be found in Table 2.3.

Table 2.3: Several studies using Ni_2P as HDO catalyst, listing of characteristics

Preparation	**Support**	**Feedstock**	**Reaction conditions**	**Main product**	**Ref.**
Imp. Phosphite	SiO_2	Dibenzofuran	200-300 °C, 30 bar H_2, fixed bed reactor	Bicyclohexane	[56]
Imp. Phosphate	SiO_2-H	Methyllaurate	300-340 °C, 20 bar H_2, fixed bed reactor	Undecane, dodecane	[57]
Imp. Phosphate	SiO_2,Al_2O_3, ZrO_2	Guajacol	300 °C, 1 bar H_2, fixed bed reactor	Catechol, benzene, phenol	[55]
Imp. Phosphate	SiO_2	Benzofuran	370 °C, 31 bar H_2, fixed bed reactor	Ethylbenzol	[58]
Imp. Phosphate	-	Methylphenol	350 °C, 44-61 bar H_2, batch reactor	Toluene, methylcyclohexane	[59]
Imp. Phosphate	SBA-15	Methyloleate	290 °C, 3-40 bar H_2, fixed bed reactor	Octadecane	[49]
Imp. Phosphate	SiO_2	Guajacol	200-300 °C, 1 bar H_2, packed bed reactor	benzene, phenol	[60]

This listing shows that mainly oxide supports and especially SiO_2 is used and the dominating preparation method is impregnation with a phosphate precursor. The biggest differences can be found in the choice of the feedstock and the reaction conditions, where various temperature and pressure conditions are used.

Other authors studied the reaction mechanism like Moon et al.,[61] who focused on the mechanism of the guajacol HDO reaction. Combined theoretical and spectroscopic studies were used to find the active centers for the HDO reaction. It was assumed that guajacol would preferentially adsorb with its OH group. Concerning this adsorption it was found that one Ni atom alone could provide an adsorption site, but three neighboring Ni atoms together would be more favorable (adsorption energy -0.23 vs. -0.50 eV). Additionally also adsorption on a P-OH group is possible. After adsorption the OH group reacts with the chemisorbed

hydrogen atoms to form water and the deoxygenated product. The chemisorption of hydrogen is therefore also a crucial reaction step. In other experiments the authors found that changing the hydrogen pressure would change the selectivity between aromatic and saturated products.

At higher pressures (8 atm vs. 1 atm) the formation of saturated compounds is favored. This is explained by the higher availability of chemisorbed hydrogen at higher pressures. The deactivation mechanisms are very similar compared to the tungsten carbide catalysts. Main deactivation pathways are particle aggregation, loss of surface area and coking. Once again the deactivation by chemical reaction is important. The Ni_2P can be oxidized and form bulk oxides or phosphides. The oxidation of P to P-OH was reported to be reversible. But also reductive deactivation by removing the phosphorus in the form of PH_3 is possible in theory.

3. Objective

The upgrading of bio-oils via HDO reaction is an important step for the supply of transportation fuels derived from lignocellulosic biomass. Compared to the industrially used hydrotreating catalysts like Co or Ni-doped molybdenum sulfides or noble metals, the transition metal phosphides and carbides possess many advantages. They are based on abundant and non-expensive elements and they do not need a continuous supply of H_2S (or other compounds) in the feed stream like the sulfide based catalysts. However, for a possible practical application, improved types of these catalysts have to be developed. Compared to other catalyst types, like noble metals, the controlled insertion of nanostructural features, for optimizing the reaction performance, is not well elaborated for transition metal phosphides and carbides.

The aim of this work is to study the synthesis methods for nickel phosphide and tungsten carbide, because the existing literature studies have shown that these two materials possess very promising activity for HDO reaction.[40][62] Several preparation routes shall be investigated and compared with each other. For the preparation of nickel phosphide, alternatives to the common impregnation-reduction method should be found and tested. The focus for the tungsten carbide synthesis will lie on the search for preparation techniques allowing a nanostructuring of this material. The preferred support material should be carbon. Not only because of the high surface areas that can be achieved with carbon based supports, but because some studies suggest that carbon may possess convenient properties regarding stability under reaction conditions.[11] Also the acidity is not very high, which could decrease coking during test reactions compared to other supports.

Concerning the carbon support it would be desirable to find methods that allow the synthesis of nanostructured material, the properties of which can be tuned. A very useful method to obtain such kind of materials is the carburization of polymer precursors. By choosing the appropriate synthesis methods, polymeric materials can be tuned regarding shape and size. Another advantage of using polymer derived carbon materials is the possibility of introducing functional groups in the polymer. This could facilitate the synthesis of the catalytic materials and improve their properties. For that reason especially polymer derived carbon supports shall be studied, regarding their capability of improving structural properties of the nickel phosphide and the tungsten carbide. This specifically holds for the important structural parameters like particle size and distribution.

4. Results and Discussion

4.1 Nickel phosphide synthesis: Impregnation

The first approach was to obtain supported Ni_2P on SiO_2 or activated carbon, by an impregnation-reduction method. This is also the most common method in literature and has proven its reliability in many examples.[54][51] In this case an impregnation solution of $Ni(H_2PO_3)_2$ in water was prepared by mixing stoichiometric amount of $Ni(OH)_2$ and H_3PO_3 through ultrasonication in the desired amount of water. The formation of $Ni(H_2PO_3)_2$ is finished when the whole amount of $Ni(OH)_2$ is dissolved, resulting in a clear green solution. In the literature also other precursor solutions are found. The most common one is a phosphate precursor where an aqueous solution of $(NH_4)_2HPO_4$ and $Ni(NO_3)_2$, yielding a nickel phosphate species, is used.[11] The main advantage of using $Ni(H_2PO_3)_2$ compared to the phosphate solution is that the phosphite can be reduced at lower temperature. This results in smaller particle sizes for the resulting Ni_2P, as higher temperatures promote particle growth and agglomeration. Using nickel hypophosphite or other similar precursors, which can also be found in literature, was not considered.[50] These materials have a low reduction temperature as well, but their reaction behaviors are not as well studied compared to the phosphite system. SiO_2 and activated carbon were used as support materials. Silica is a frequently used support for Ni_2P and serves in this case as a test and reference catalyst. Activated carbon was used to show basically, if Ni_2P can be synthesized on a carbon support to evaluate eventual difficulties or hindrances, because the next step would be the use of structured carbon supports. The support materials were impregnated with the desired amount of $Ni(H_2PO_3)_2$ dissolved in the incipient wetness volume for the corresponding substrate. The dried substrates were then reduced in 10% H_2/Ar and heated to 400 °C where the temperature was kept for 3 h followed by heating to 500 °C and the latter temperature was kept for 2 h. The reduction conditions were adapted from Cecilia et al.[51] who investigated the formation of Ni_2P under different conditions by using a phosphite precursor. This study showed that at 500 °C the Ni_2P formation could be completed in the applied time. Although the dwell time at 400 °C was not necessary for the Ni_2P formation in this case, it was applied to ensure comparability with other materials, where this dwell time was essential. Catalysts with three different loadings of 5, 10 and 15% were synthesized in each case on SiO_2 and activated carbon.

The formation of Ni_2P was controlled with XRD measurements. In Figure 4.1 the diffractograms for the 10% Ni_2P on SiO_2 and activated carbon are depicted.

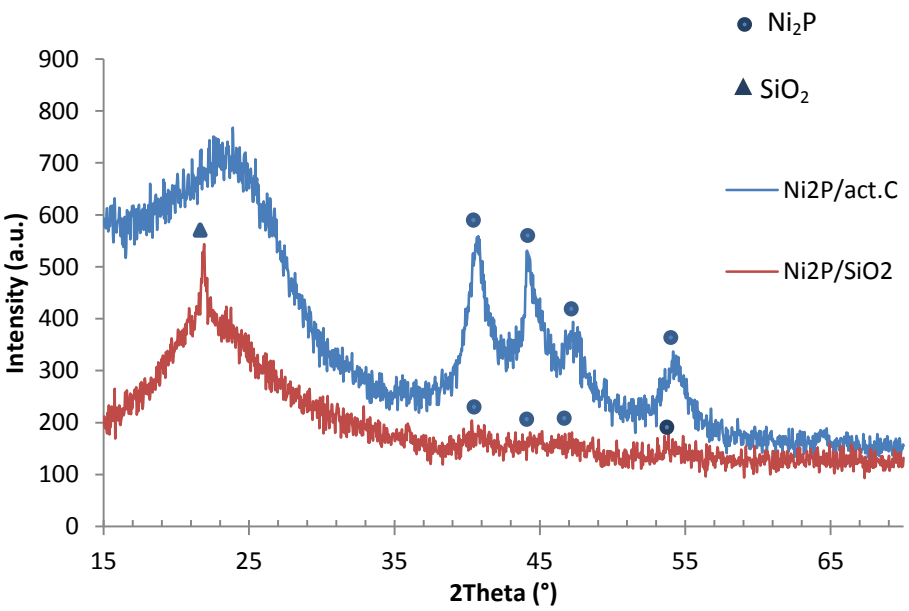

Figure 4.1: X-Ray diffractograms of 10%-Ni_2P/SiO_2 and 10%-Ni_2P/act. C

For the carbon supported Ni_2P the diffraction peaks at 40.7, 44.6, 47.3 and 54.3 ° are clearly visible and therefore Ni_2P can be identified as the only detectable phase. The pronounced peak broadening indicates that the formed phosphide particles are relatively small. The broad peak between 20 and 30 ° can be attributed to the carbon support. In contrast, the Ni_2P peaks for the SiO_2 supported material are hardly observable. Nevertheless, very slight indications at the angles characteristic for Ni_2P can be identified. These reflections also show a broadening similar to the carbon supported material. However, the question remains, why the peaks are very well visible on the carbon support but hardly identified on the SiO_2 support. This may be attributed to the different X-ray permeability of the two support materials. Carbon is a light element; hence its X-ray absorption is weaker than for the heavier SiO_2. This could cause the weakening of the diffraction signal and explain the difference in the observed peak intensities. However, the Ni_2P particles may also be smaller and/or more defective on the SiO_2 which would lead to broader, less intense reflections. In the silica supported material an additional peak can be found at 22.0 ° which is attributed to the cristobalite modification of SiO_2. It probably derived from the amorphous silica through the high temperature treatment. The determined BET surface and pore volume show a decrease with increasing Ni_2P loading (Table 4.1). This tendency was also observed in literature and can be ascribed to the growing amount of particles in the support material which are blocking more and more pores and thus decreasing the surface area and the total pore volume. [51] Additionally it has to be considered that the loading of Ni_2P causes a weight gain of the material. At the same time the additional surface area, deriving from the

phosphide, is not known. Therefore it should be considered that the weight gain could probably influence the results of the BET surface area measurements.

Table 4.1: Textural properties of impregnated Ni_2P/SiO_2 or act. carbon catalysts

	SiO_2		act. carbon	
Ni_2P [%]	BET [m^2/g]	pore Volume [cm^3/g]	BET [m^2/g]	pore Volume [cm^3/g]
0	500.24	0.750	1300.0	1.100
5	279.27	0.562	826.30	0.868
10	274.39	0.529	797.63	0.824
15	225.05	0.477	678.37	0.681

A drawback of the impregnation method is that the distribution and the particle size of the Ni_2P cannot be influenced or controlled. A better distribution and smaller as well as more monodisperse particles can be achieved by the control of the support design. The suitable support material for this is carbon, and there are different ways how nanostructured carbon supports can be produced. In this work a soft-templating method is used to produce hollow polymer shells which can then be carbonized to yield hollow carbon shells that serve as support material. The used polymer possesses a resorcinol resin-like structure and can be prepared by polymerization of 2,4-dihydroxybenzoic acid and formaldehyde (in this case hexamethylenetetramine was used as formaldehyde precursor) in aqueous solution. The shaping of the polymer into hollow shells is accomplished by using a surfactant mixture of sodium oleate and Pluronic® P123. By changing the surfactant:water ratio the size of the resulting hollow shells can be tuned. It was decided to use a shell size of approx. 200 nm. The final hollow polymer shells (HPS) were obtained after a one step autoclave synthesis. This shows clearly the advantage of using surfactants as soft templates, which can be just washed away and do not need an additional reaction step for leaching or removing. The use of 2,4-dihydroxybenzoic acid allows the introduction of free carboxylic acid groups into the polymer. The acid groups work like in an ionic exchange resin and by interacting with the nickel ions, the polymer is loaded with them. This should ensure a good distribution of the final Ni_2P particles. The structure of the polymer is schematically shown in Figure 4.2.

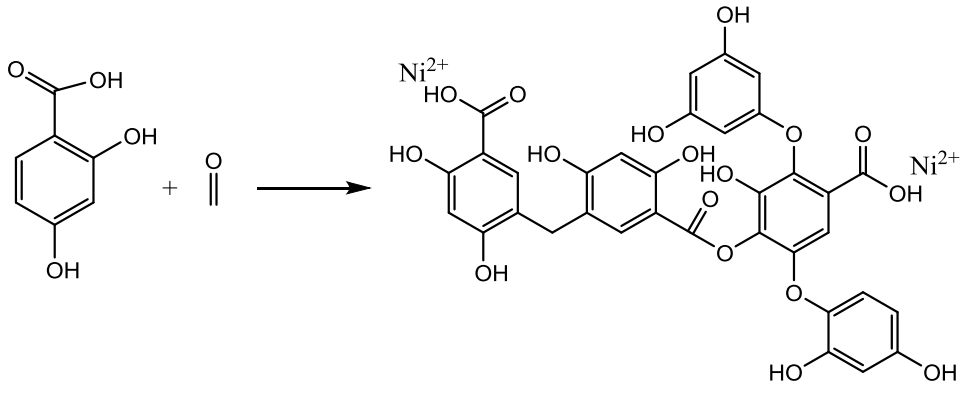

Figure 4.2: Polymer structure of HPS

After the polymer shells had been synthesized, they were impregnated with the $Ni(H_2PO_3)_2$ solution and underwent the same reduction treatment in the tubular furnace like the SiO_2 and activated carbon supports. The carbonization of the polymer support and the Ni_2P formation occurred simultaneously and the XRD measurements confirmed that Ni_2P was again the only formed phase. What had to be taken into account was the weight loss during the carbonization process which accounted for approx. 50% of the polymer support. Thus the amount of $Ni(H_2PO_3)_2$ solution had to be adapted. For reasons of comparison also another impregnation method was applied. Here the unloaded hollow polymer shells were at first carbonized to yield hollow carbon shells (HCS). These carbon shells were then impregnated with the phosphite solution and reduced at 500 °C. Again, three catalysts with three different Ni_2P loadings, namely 5,10 and 15% were produced for each support. The textural properties were investigated and are shown in Table 4.2.

Table 4.2: Textural properties of impregnated Ni_2P/HPS or HCS catalysts

	hollow polymer shells		**hollow carbon shells**	
Ni_2P [%]	**BET [m^2/g]**	**pore Volume [cm^3/g]**	**BET [m^2/g]**	**pore Volume [cm^3/g]**
0	540.00	0.390	540.00	0.390
5	443.81	0.410	391.94	0.453
10	404.82	0.546	361.67	0.459
15	308.46	0.485	306.83	0.529

It can be seen that also on these supports the BET surface area decreases with increasing Ni_2P loading, whereas the pore volume does not exhibit a traceable trend. The materials derived from the impregnation of the polymer shells also show a higher BET surface area compared with the impregnated carbon shells. The materials were further investigated with transmission electron microscopy (TEM), which can deliver additional information to explain the difference in the BET surface area.

The TEM pictures in Figure 4.3 show that the hollow shell structure of both materials is not altered by the carbonization and reduction process. The polymer and carbon shells can be differentiated by their diverging contrast, whereas the Ni_2P particles are clearly visible on the inside and the outside of the shells. The use of polymer or carbon shells as support results in a slightly different structure and assembly of the Ni_2P particles. When polymer shells are used as support, the final material shows mostly only one round Ni_2P particle incorporated in a single shell. The phosphide particles are quite monodisperse and have a size of 10-15 nm. By using carbon shells the Ni_2P particle distribution is changed. Two fractions of particles can be identified. A smaller fraction with a particle size of approx. 5 nm and a bigger fraction containing particles sized up to 20 nm and more. Additionally the bigger particles are not regularly shaped and located preferentially on the outside of the carbon shells. These results can be explained by the different textures and morphological characteristics of the two

supports. The comparably soft polymer shells change their texture considerably, when they are converted to carbon shells during the temperature treatment. The phosphite solution is soaked in all-over the single shells and forms a Ni_2P particle in the inside of the shell, which is at the same time converted to carbon during the heat treatment. On the other hand, the impregnated carbon shells have already a rigid structure which is not altered during the additional temperature treatment. This rigid structure might hinder the full soaking of the phosphite precursor into the support, which results in the bigger Ni_2P particles at the outside of the shell. The part of the phosphite solution that was better distributed and could also infiltrate the shell structure formed then the smaller particles.

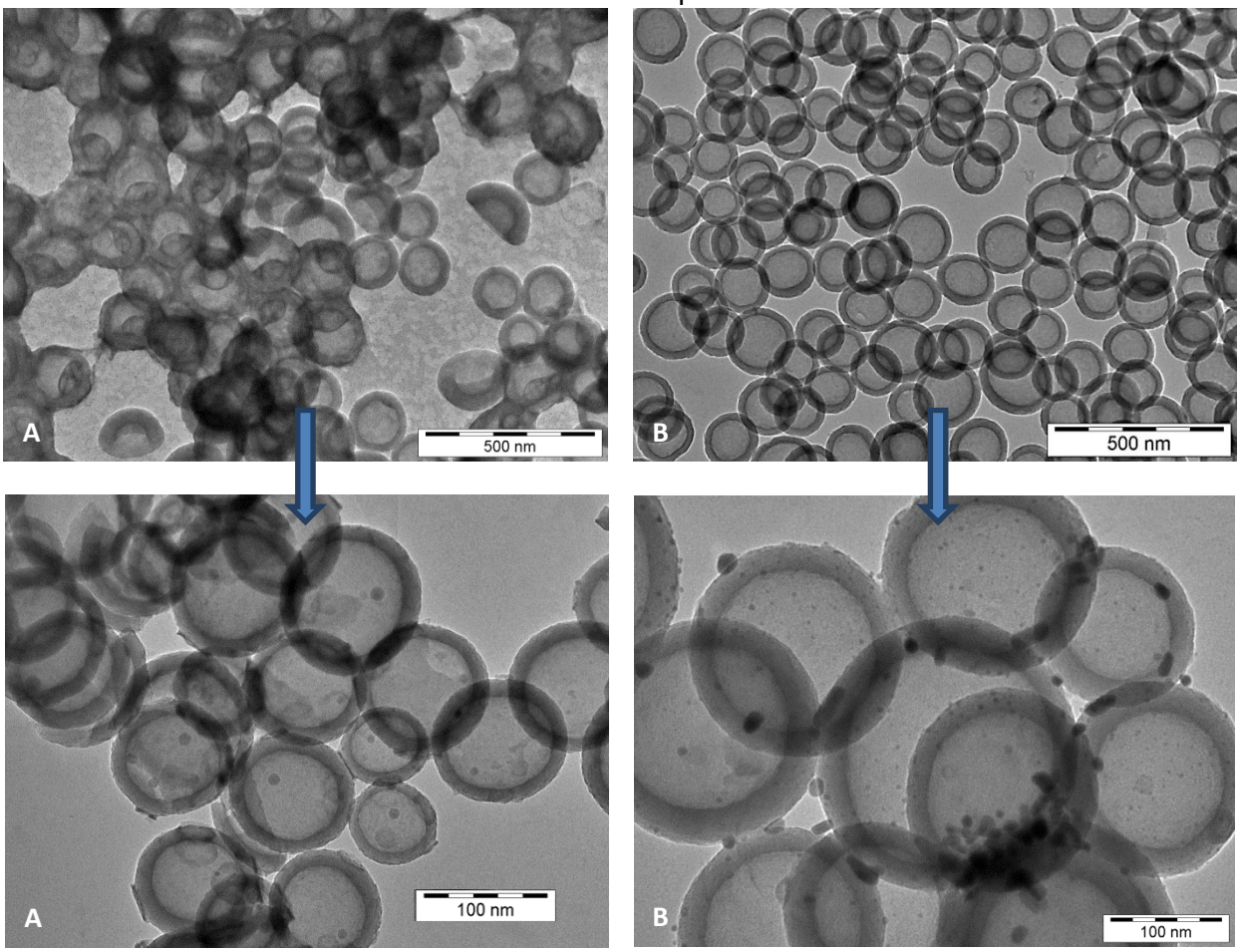

*Figure 4.3: TEM micrographs of 10%-Ni_2P/HPS (**A**) before loading and carbonization and 10%-Ni_2P/HCS (**B**) pre-carbonized, before and after loading*

The difference in the BET surface area between the two material types may be attributed most likely to the double thermal treatment of the impregnated carbon shells. At first they were heated to obtain the unloaded carbon shells and then they were heated again after impregnation with the phosphite solution, to obtain the Ni_2P particles. Thermal stress is a common reason for lowering of BET surface and so the repeated thermal treatment is a very likely explanation for the observed phenomenon.

Anyhow, both catalysts do not show all characteristics that were requested for these materials. The dispersion of the Ni_2P particles is for both materials not high enough. For the polymer impregnated material the particle size of approx.15 nm should be improved and for the carbon impregnated one the polydispersity of the particles is a challenge. Obviously the additional carboxylic groups in the polymer cannot effectively distribute the Ni_2P particles when the nickel cation and the phosphite anion are present at the same time. Hence a further development of the synthesis methods was necessary.

4.2 Nickel phosphide synthesis: Direct phosphidation

An alternative method would be the conversion of metallic nickel particles directly to nickel phosphide. This pathway has the advantage that the particle size and distribution of metallic nickel particles can be well controlled, and also the interactions between the nickel ions and the phosphorus containing anions, which complicates the process, can be avoided. The first step was the deposition of the metallic nickel particles onto the hollow shell support. For this task a synthetic protocol from Hyeon et al.[52] was adapted for our requirements, by changing the amount of used reactants and using supported and not free nickel particles. This method should allow the production of monodisperse nickel particles with a size of approx. 5 nm. The hollow carbon shells were used as support material, because the polymer shells might not withstand the high temperature reaction conditions. Characterization with XRD and TEM showed that metallic nickel particles with a size of approx. 6 nm were formed. Then the metallic nickel had to be converted into nickel phosphide. In the literature there exist several synthetic protocols that appeared to be suitable for this task.[53] All of these require high temperature conditions (min. 300 °C) and a phosphorus containing compound delivering the phosphorous that can then be inserted into the nickel lattice. It was decided to use trioctylphosphane (TOP) as phosphorus carrier, because it is a non-toxic liquid which has certain advantages compared to the highly toxic phosphane gas which can also be used for this reaction. By using TOP, the metallic nickel was completely converted to Ni_2P, and no signals of the metal or other phosphide phases could be detected in the X-ray diffractograms (Figure 4.4). Again three different loadings of Ni_2P with 5, 10 and 15% were realized. The samples synthesized by this method are denoted in this work as *XX% Ni_2P/HCS – direct*.

Before the analysis results of these materials are shown, the synthesis method for a comparable material is discussed. Besides of using the unloaded carbon shells as support, the polymer shells were directly used as support for the direct phosphidation reaction. That means the first step is the deposition of metallic nickel particles. Therefore the hollow polymer shells were suspended in an aqueous solution of nickel nitrate to load the support with nickel ions. After drying, the loaded polymer shells were reduced under a mixed H_2/Ar atmosphere in a tubular furnace. Here the amount of hydrogen had to be adjusted carefully. As metallic nickel is an excellent hydrogenation catalyst, it will hydrogenate its own polymer or carbon support and when the ratio of hydrogen in the gas stream is too high, a major part

of the support material will be lost. This causes challenges with calculating the desired metal loading and with reproducibility. To ensure a reproducible weight loss of the support, the hydrogen ratio should not exceed 5%, especially when reducing materials with high metal loading. The reduction treatment yields again nickel-loaded carbon shells, which undergo the direct phosphidation procedure with TOP at high temperature (300 °C). The subsequent XRD measurement confirmed again the full conversion of the metallic nickel and Ni_2P was the only detected phase (Figure 4.4). The samples synthesized with this method are denoted as *XX% Ni_2P/HPS – direct*.

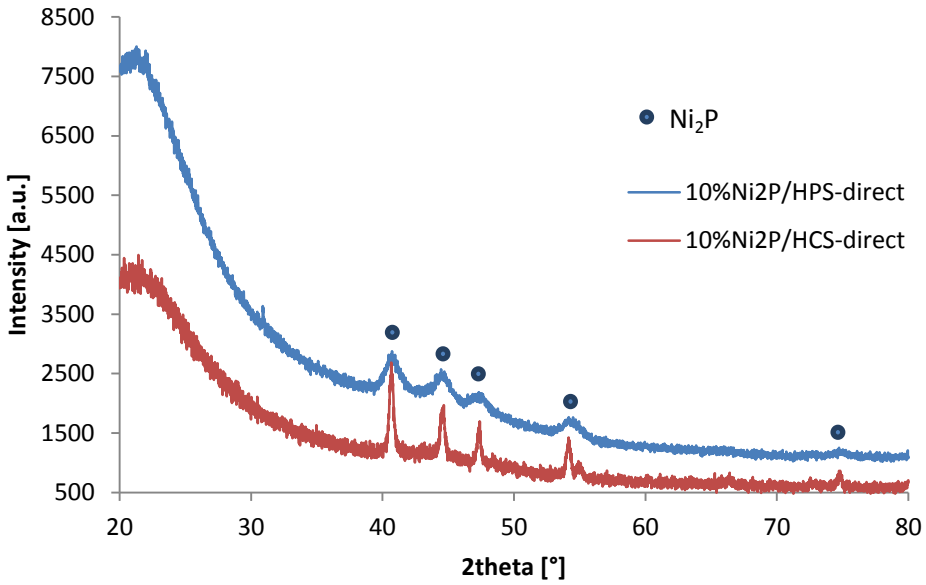

Figure 4.4: X-Ray diffractograms of 10%-Ni_2P/HPS - direct and 10%-Ni_2P/HCS - direct

When the material (*10%-Ni_2P/HPS – direct*) was characterized by nitrogen physisorption, unexpected results were obtained. The value for the BET surface area was only 33.9 m^2/g, which was unexpectedly low for these types of materials. The sorption isotherms for the "*10%-Ni_2P/HPS – direct*" (Figure 4.5) suggested that, this material did not possess any porosity anymore. The measured isotherms indicate non porous particles with a high interstitial pore volume. To find the reason for this behavior the TEM micrographs of this sample (Figure 4.6) were closely investigated, but no conspicuity was found. The carbon shell support showed no obvious changes like collapse of the hollow shell or signs of sintering. Also the particle distribution showed the expected appearance. As no obvious textual transformation or abnormity could be identified, the most likely possibility was that the pore structure has been blocked by a compound that was not visible in the TEM pictures. Hence the reason for this pore blockage must be caused by the synthesis conditions. When the metallic nickel particles are converted to Ni_2P at high temperatures, trioctylphosphane is used as reagent and dioctylether as solvent. They could infiltrate the pore system of the carbon shells and therefore block all the pores, because with a boiling point of 286 °C (1 bar) for the dioctylether and 290 °C (0.07 bar) for the TOP, the activation temperature of 200 °C

prior to the sorption experiments would not be sufficient to evaporate the compounds, particularly when it is trapped in the pore system and the capillary forces would even stronger supress the evaporation. To prove this hypothesis, the phosphidized sample was heated under flowing Ar to 500 °C for 2 h. Then the sorption experiment was repeated and the measured BET area was 439 m^2/g for the "*10%-Ni_2P/HPS – direct*" material, which is a much more realistic value. The obtained isotherm (Figure 4.5) resembles a type 4 isotherm which indicates a mesoporous structure of the material. So the reason for the low surface area in the first measurement pore blocking by TOP and even extensive washing with ethanol after the reaction could not remove it. An activation step is thus required to produce a material suitable as catalyst. However, this temperature treatment is no disadvantage of this synthesis method. When using the material as catalyst they have to be reactivated again anyway under high temperature and reductive conditions. It has, however, to be considered in the reactivation protocol that also the remaining TOP should be removed, and thus the activation process has to be adapted to meet this requirement.

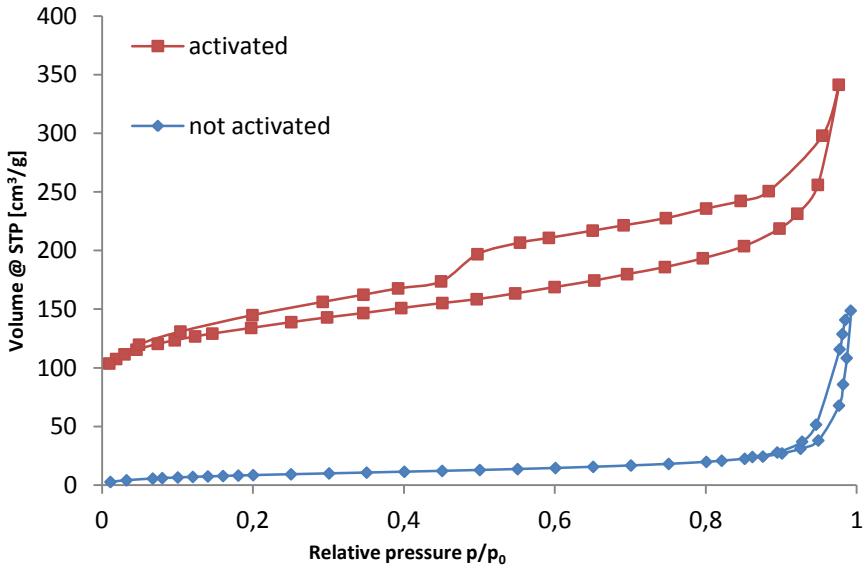

Figure 4.5: Sorption isotherms of "10% Ni_2P/HPS – direct" before and after heating in an argon stream.

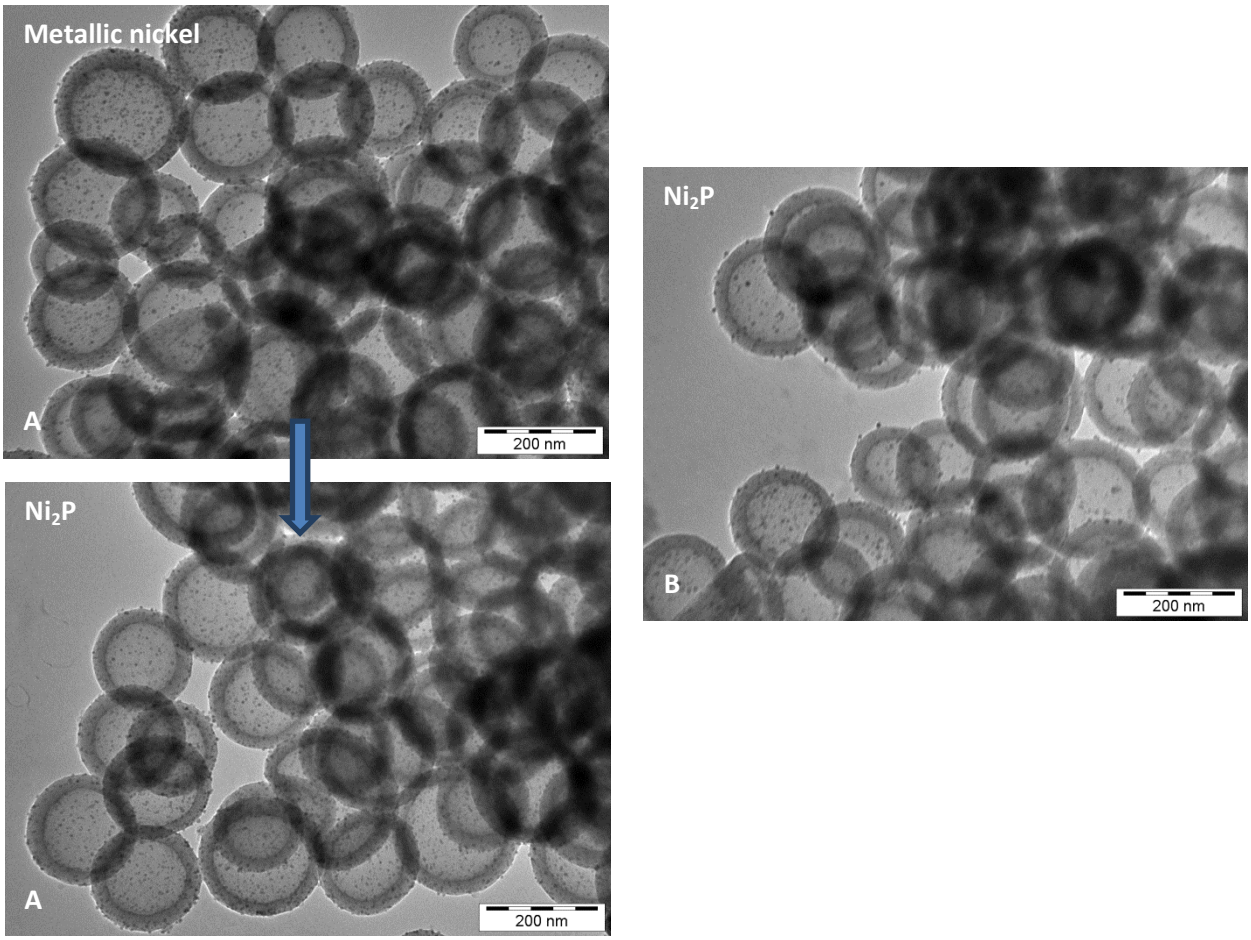

Figure 4.6: TEM micrographs of 10% Ni_2P/HPS – direct (A) and 10% Ni_2P/HCS – direct (B)

TEM micrographs clearly reveal that the direct phosphidation reaction does not lead to a significant increase in the particle size. The particle sizes of the metallic nickel and the nickel phosphide were determined for the HPS derived material and the sizes were 4.4 ± 1.2 nm for the metallic nickel and 4.8 ± 1.5 nm for the phosphide particles. Comparing the two materials from the HPS and the HCS route, they show many similarities, such as the good distribution and the homogeneity of the phosphide particles and the relatively small particle size. Thus, the main demands that had originally been formulated for the catalysts could be met. This is a basic advantage of the direct phosphidation method compared to the impregnation method, as by the latter method one could not achieve comparable distributions and particle homogeneities. Focussing again on both materials obtained from the direct phosphidation, also some differences can be found, in addition to the similarities. The HPS derived material has a slightly lower particle size, and also the particle size distribution is more homogeneous for this type of materials. This fact is proven by evaluation of the particle size distributions for both materials which are depicted as histograms in Figure 4.7.

Table 4.3: Particle sizes of 10% Ni_2P/HPS – direct and 10% Ni_2P/HCS – direct

	HPS - direct	HCS - direct
particle size	4.9 ± 1.5 nm	6.7 ± 2.3 nm

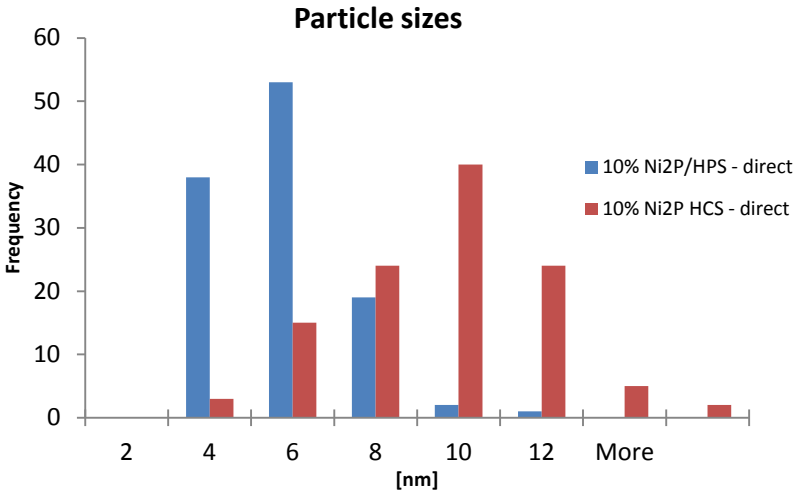

Figure 4.7: Histogram particle sizes of 10% Ni_2P/HPS – direct and 10% Ni_2P/HCS – direct

In Table 4.4 the BET surface areas and pore volumes for the three different loadings of each material are shown. What can be seen is again the decreasing BET surface area with higher loading. Similar to the previous method also here the BET surface area is higher for the materials derived from the polymer shells. The most likely reason for this fact is again the double thermal treatment of the carbon shells.

Table 4.4: Textural properties of directly phosphidized Ni_2P/HPS or HCS catalysts

	hollow polymer shells -direct		hollow carbon shells - direct	
Ni_2P [%]	BET [m^2/g]	pore Volume [cm^3/g]	BET [m^2/g]	pore Volume [cm^3/g]
5	440,55	0,826	400,11	0,634
10	439,83	0,528	405,44	0,541
20	389,35	0,675	388,08	0,458

As the HPS based materials showed more favorable structural properties, they were investigated more closely by TEM. This led to a remarkable observation. When comparing the TEM micrographs of the two materials with calculated Ni_2P loading of 10% and 20% the increase in the number of individual visible particles was not as high as would be expected from the doubled loading. Additionally, a fraction of bigger particles with a diameter of approx. 40 nm could be found. These big particles were not present in the materials with a loading of 5% or 10%. This can be interpreted as follows: The distribution of the Ni_2P particles is caused by the free carboxylic groups in the polymer shells. They interact with the nickel ions, and so monodisperse and small metallic nickel particles are created that are subsequently converted to the Ni_2P. When the nickel loading is increased, not enough free carboxylic groups are in an appropriate distance to ensure a good distribution of the

particles. This causes particle agglomeration and might explain the formation of bigger particles in the highest loaded sample. The TEM micrograph in Figure 4.8 shows this sample, where beside the well dispersed small Ni_2P particles with a size of 5 nm also the big agglomerated ones with a size of 40 nm can be identified.

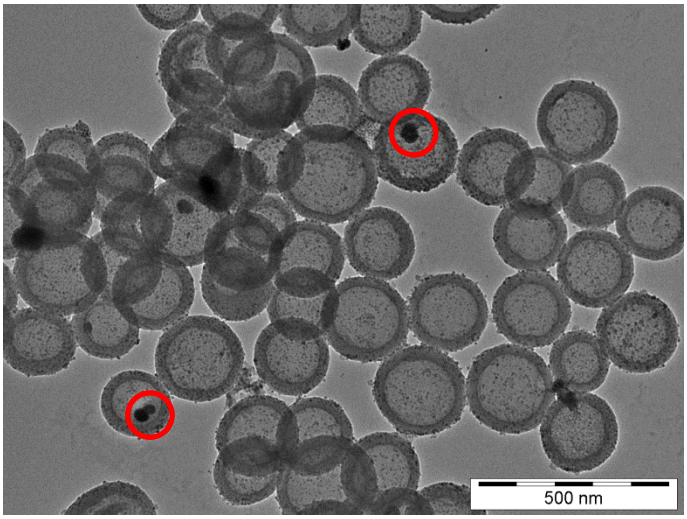

Figure 4.8: TEM micrograph 20% Ni_2P/HPS – direct

Determining the particle size only with TEM can sometimes lead to misinterpretations as only a very small part of the sample is actually investigated. To verify the particle sizes measured in the micrographs, small angle X-ray scattering (SAXS) measurements were performed. The results from these measurements confirm the sizes measured from the TEM micrographs. In Table 4.5 the values for the particle sizes, determined by TEM and by SAXS, are shown. Here only the results for the *20% Ni_2P/HPS – direct* sample are shown, to illustrate that also 2 different size fractions of particles can be determined by SAXS. Therefore the scattering curve of the loaded HCS is measured between 0.5 and 5 °and then the curve of the unloaded shells is subtracted from this curve.

Table 4.5: Particle sizes of 20% Ni_2P/HPS – direct determined by TEM and SAXS

TEM	**SAXS**
4.9 and 45 nm	5.1 and 41.9 nm

For further investigation an elemental analysis to determine the nickel and phosphorous content in the material was conducted. This analysis suggested that the actual loading of Ni_2P for the materials was lower than the calculated one, especially for the higher nominal loadings. For this observation again the number of free carboxylic acid groups could be a possible explanation. Since the nickel is introduced by ion exchange in aqueous suspension, the amount of free carboxylic acid groups determines the amount of nickel that is loaded onto the substrate. As the number of acid groups is fixed, there is the chance, that for higher nickel loadings the number of free carboxylic acid groups is insufficient to take up the whole

amount of nickel. Hence the nickel loading capacity is limited and shows a saturation behavior which is also supported by the elemental analysis. The higher the nominal loading, the higher is the difference to the actual loading. Only for the 5% loading the nominal and the actual loading are consistent. For the 10% loading there is already an aberration that has to be considered and for the 20% nominal loading there is a major difference.

Table 4.6: Nickel and phosphorous content of Ni_2P/HPS – direct material

nominal Ni_2P loading [%]	**Ni [%]**	**P [%]**	**actual Ni_2P loading [%]**
20	8,7	3,6	12,3
10	5,3	2,8	8,1
5	3	1,5	4,5

It can be concluded that both synthesis pathways lead to a material with very good distribution of monodisperse and small particles. What must be taken into account is the limited nickel loading capacity when choosing the polymer shells as support. Probably the highest Ni_2P loading that can be achieved by loading of the HPS support is approx. 10%. If higher loadings are desired the carbon shells should be used as support material, even if the corresponding synthesis method yields slightly bigger particles which are not that well dispersed.

4.3 Tungsten carbide synthesis: Hollow carbon shell support

The other goal of this work was to produce a carbon supported tungsten carbide material. Also here a nanostructured support should be used to study the properties of the tungsten carbide on such a support material. Compared to the phosphide species, the variety of different synthesis methods for carbide formation on a support is relatively small. By far the most widely used synthesis method is the impregnation method.[10] A support material is impregnated with a tungsten precursor which is then converted into carbide. For the carbidization process there exist only a few possibilities. Here it is intended to form the tungsten carbide via the carbothermal reduction pathway.[44] In this synthesis method the carbon for the carbide formation is not delivered by a carbon containing gas like methane but directly by substrate. Therefore this method only works with carbon substrates. The method is tested by producing tungsten carbide on an activated carbon support. The activated carbon is impregnated with an aqueous solution of ammoniummetatungstate until incipient wetness and then reduced under pure hydrogen atmosphere at 800 °C. The XRD analysis showed that W_2C was formed as the only detectable crystalline phase. The reflections at 34.4, 38.0, 39.5, 50.3, 61.8, 69.7 and 74.9 ° can be attributed to the W_2C phase (Figure 4.9). After treatment at lower temperatures no reflections corresponding to tungsten carbide were visible in the XRD patterns. As a next step it was attempted to form the tungsten carbide on the nanostructured carbon support. Therefore the hollow carbon shells were impregnated

with the ammoniummetatungstate solution and also heated to 800 °C in hydrogen atmosphere. Again the XRD analysis indicated the formation of W_2C.

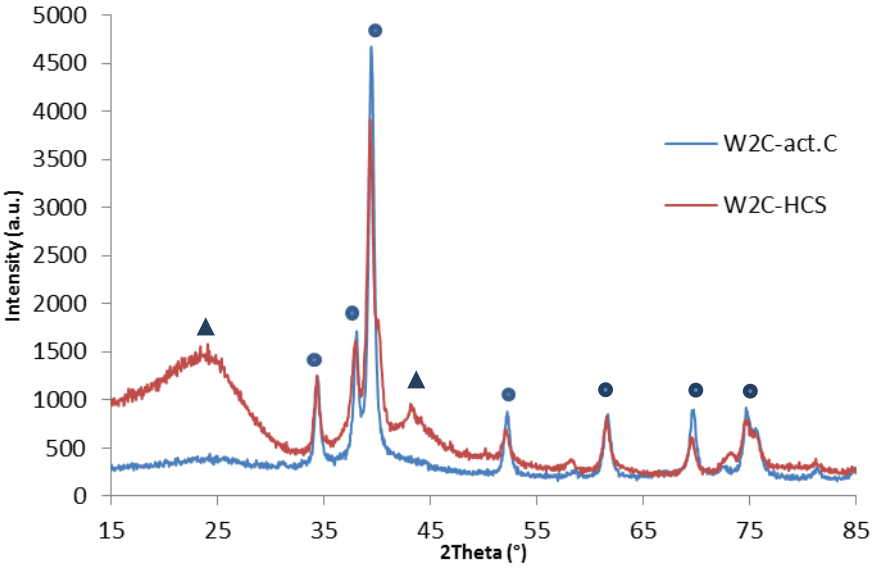

Figure 4.9: X-ray diffractograms of 20% W_2C/act. C and 5% W_2C/HCS

Besides the characteristic peaks for the W_2C phase, which were also found for the activated carbon supported material, two broad features at 15-25 ° and 40-45 ° are present in the HCS supported carbide. The peak at 15-25 ° is characteristic for carbon and is found in all kinds of carbon materials, whereas the peak at 40-45 ° is only sometimes found in HCS supported material. Nevertheless, this peak can also be attributed to carbon. The HCS supported material was also investigated with TEM and it can be seen from the micrographs (Figure 4.10) that the carbon shell support is damaged and shows signs of decomposition. It seems that the high temperatures and the pure hydrogen atmosphere are too aggressive for the carbon shells.

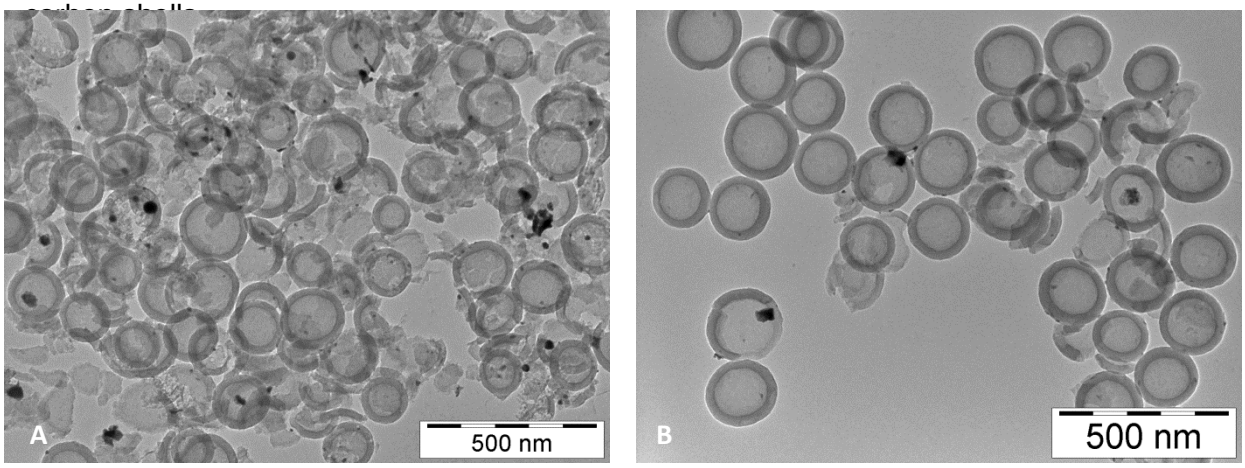

Figure 4.10: TEM images of 5% W_2C/HCS, in which the degradation of the carbon shells can be seen

The carbide formation takes place by insertion of carbon atoms from the support into the tungsten lattice. If too much carbon is required for the carbide formation this may locally lead

to degradation of the support. Another very likely explanation is that W_2C is an active hydrogenation catalyst, and under these reaction conditions it can hydrogenate its own carbon support which is thereby converted to methane. From the TEM it is obvious that certain areas of the shells were degraded, and only parts of the shells are left over. The distribution of the W_2C particles is very inhomogeneous and also the particle sizes are polydisperse. The employed synthesis protocol thus does not allow tungsten carbide formation at a lower temperature and without decomposing the support material. It was tried to overcome this challenge by feeding ethane in the gas stream during synthesis. According to the literature the carbidization with ethane takes place faster than with methane.[43] The hope was that the carbon from the gas phase would be incorporated faster in the tungsten lattice than the carbon from the support, thus loss of carbon could be lowered. However, the TEM investigation shows (Figure 4.10 (B)) the same signs of degradations. Therefore it can be concluded that the tungsten carbide hydrogenates its own carbon support and the carbon depletion of the support is not the main reason for degradation. Besides the degradation of the support also the inhomogeneous distribution of the carbide particles is a problem. Also impregnating the polymer shells instead of the carbon shells did not solve this problem, as the resulting material showed the same decomposition and distribution issues. The lesson learned from these experiments is that neither the hollow polymer shells nor the carbon shells are suitable supports for well dispersed and small sized tungsten carbide. The outer wall of the carbon shells is too thin to withstand the hydrogenating conditions and is decomposed. Furthermore the carboxylic acid groups cannot ensure an adequate distribution of the tungsten carbide particles. The reason for this is the anionic nature of the acid groups. The tungsten precursors are all anionic species in aqueous solution. Thus, there are no attractive but repulsive interactions between the tungsten precursor and the carboxylic acid groups what prevents a good distribution of the resulting particles. To solve these challenges, another support material has to be found that can ensure a better distribution and has also a different shape which is not that susceptible to decomposition.

4.4 Tungsten carbide synthesis: Nitrogen doped structured carbon

The nanostructuring of the carbon support by shaping a polymer precursor was a successful strategy for the nickel phosphide materials and shall therefore be kept. The next step was to find an appropriate polymer precursor with different chemical functionality. To facilitate the distribution of the anionic tungsten precursors, cationic functional groups should be introduced into the polymer material. An effective way to accomplish this task is the incorporation of nitrogen into the material by changing the monomers of the polymer. Instead of the carboxylic acid containing monomer, 1,3-aminophenol is used to form the resorcinol like network with formaldehyde (again hexamethylenetetramine is used as precursor). In acidic environment the nitrogen containing groups are protonated and should thus enable a better distribution of the tungsten oxide polyanions. The proposed chemical structure of the polymer is depicted in Figure 4.11.

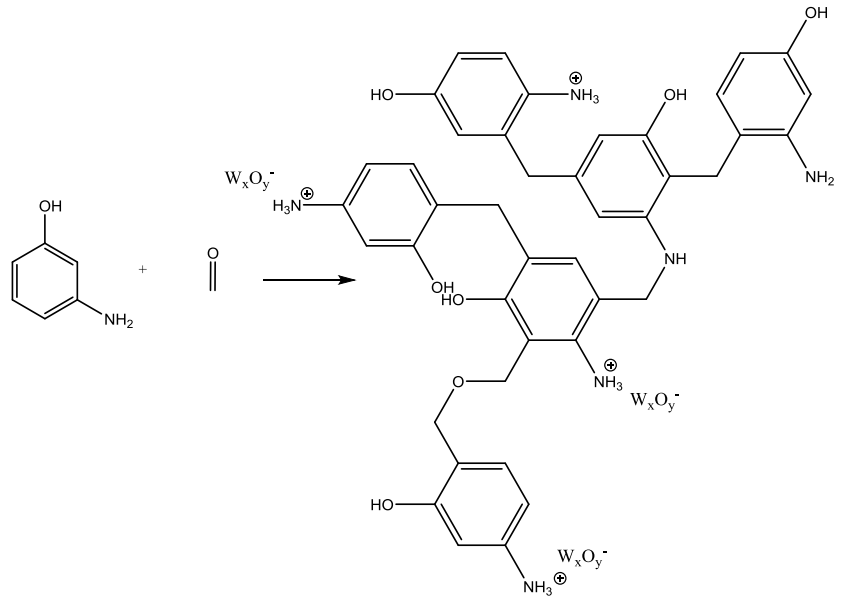

Figure 4.11: Proposed structure for nitrogen containing resorcinol like polymer

The second drawback of the carbon shell support was the hollow shell structure could not withstand the reductive conditions at high temperatures and was thus decomposed. So the other modification of the polymer support concerns the shape of the final particles. Instead of the fragile hollow shell structure a more rigid structure should be produced. Thus, round particles with an ordered pore structure to retain the high surface area were targeted. To change the particle shape, the surfactant mixture serving as a soft template has to be altered. For this nitrogen-containing polymer the used soft template was Pluronic® F127. By using this surfactant, polymer spheres with a structured pore system could be synthesized. The variation of the surfactant concentration in the aqueous solution resulted in differently sized polymer spheres. Finally a surfactant concentration was adjusted to receive polymer spheres with a size of approx. 200 nm. The as-received polymer spheres were loaded with tungsten by dispersing the spheres in an acidic (for protonation of the nitrogen groups) aqueous ammoniummetatungstate solution. The dried, loaded polymer spheres underwent then a thermal treatment under different atmospheres to carbonize the support, and simultaneously the carbide should be formed. Several reaction conditions were applied and gave different results. Treatments under pure hydrogen atmosphere led to a total decomposition of the material, so the gas was changed to argon as carrier gas with a hydrogen fraction of 20-50%.

A thermal treatment at 700 °C under a 50% H_2/Ar atmosphere could preserve the carbon support, visible in the TEM micrograph (Figure 4.12). These micrographs show the mesoporous structure of the carbon spheres and the texture of the surface, caused by the pores. Compared to the hollow shells these nitrogen-doped spheres exhibit a more dense structure. The change of the soft-template has therefore served its purpose. The TEM micrographs show also particles with a size of 3.4 ± 1.4 nm. The investigation of the observed particles proved that the incorporated nitrogen was able to disperse the tungsten

species. Hence the resulting particle distribution is much better than on the HCS support. The surface area of this material is 355 m^2/g, which is considerably lower than the 472 m^2/g for the unloaded carbon spheres. However, the high temperature treatment makes a certain loss of surface area inevitable. Again the mass increase through the tungsten loading must not be neglected.

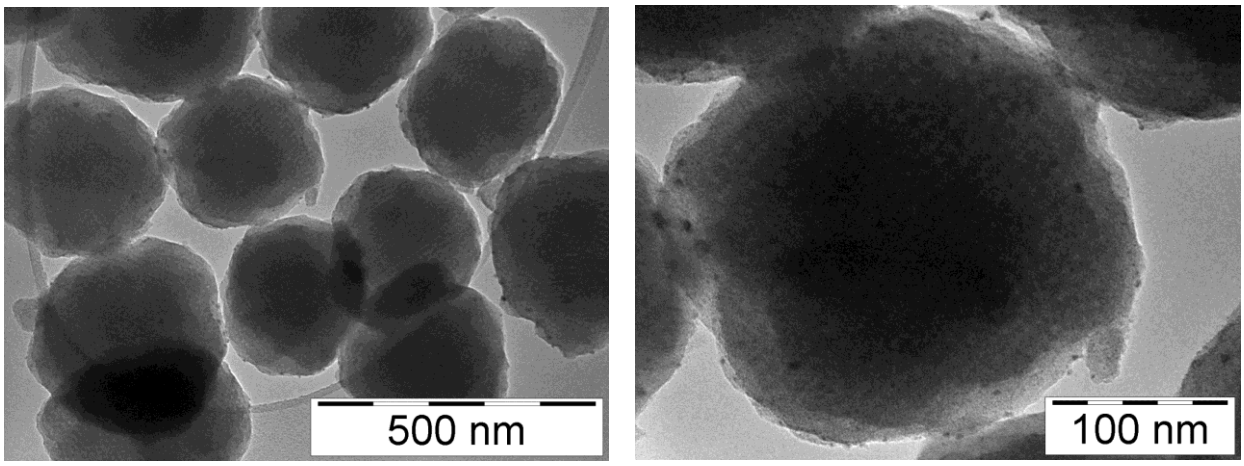

Figure 4.12: TEM micrograph of W-loaded nitrogen-doped carbon spheres, reduced at 700 °C in 50 % H_2/Ar

The material was further investigated by XRD to determine the phase of the formed particles and the reflections in the diffractogram (Figure 4.13) can be assigned to a tungsten-oxy-carbide species. This $W_2(C,O)$ species is an intermediate in the carbide formation. The possibility that the $W_2(C,O)$ would result from a subsequent oxidation of the possibly already formed carbide is not very likely, because this was not observed in the previous experiments on other carbon substrates. Furthermore a hypothetical oxidation would form only surface oxide species, whereas the observed $W_2(C,O)$ is a mixed oxy-carbide including also the inner part of the particles. Thus it can be assumed that at 700 °C the carbide formation is only starting, but cannot be completed due to the low temperature. Keeping the sample for a longer time at 700 °C (6 instead of 3 h) did not change the result. So the low temperature did not allow the carbon from the support to completely diffuse into the tungsten lattice to form the carbide. As alternative pathway gas phase carbidization was therefore investigated. Ethane was added to the mixed H_2/Ar stream at 700 °C as it was assumed that the carbon from the ethane could easier infiltrate the tungsten lattice. However, this assumption was not confirmed. The XRD measurements (not shown here) confirmed again only the formation of the oxy-carbide. An additional problem was realized when the BET surface area of this material was measured, because the determined surface area was only 18.9 m^2/g and no porosity was detected. As the TEM micrographs (not shown here) did not illustrate any conspicuity, the most likely explanation for this observation was that the ethane decomposed to carbon inside the pore structure of the carbon spheres, which blocked the complete pore system. It would be very difficult to remove the deposited carbon from the porous structure. Due to these drawbacks no further gas phase carbidization experiments were conducted.

Nevertheless, the previous experiments indicate that for a complete carbidization, a higher temperature is needed. The same material was thus at first heated to 600 °C under pure argon atmosphere to carbonize the polymer support, thereby the carbonization process is separated from the carbidization, which is conducted afterwards by heating to 800 °C under a pure H_2 atmosphere. Only the previous carbonization could prevent the decomposition of the material under the pure H_2 atmosphere at those temperatures. It can be seen from the X-ray diffractogram that now W_2C is the only detected phase (Figure 4.13). The reflections are sharper, which is a hint that the size of the particles increased due to the high temperature treatment. To obtain the smallest possible particle size and total carbidization at once, the time for the temperature treatment and the best H_2/Ar ratio have still to be optimized.

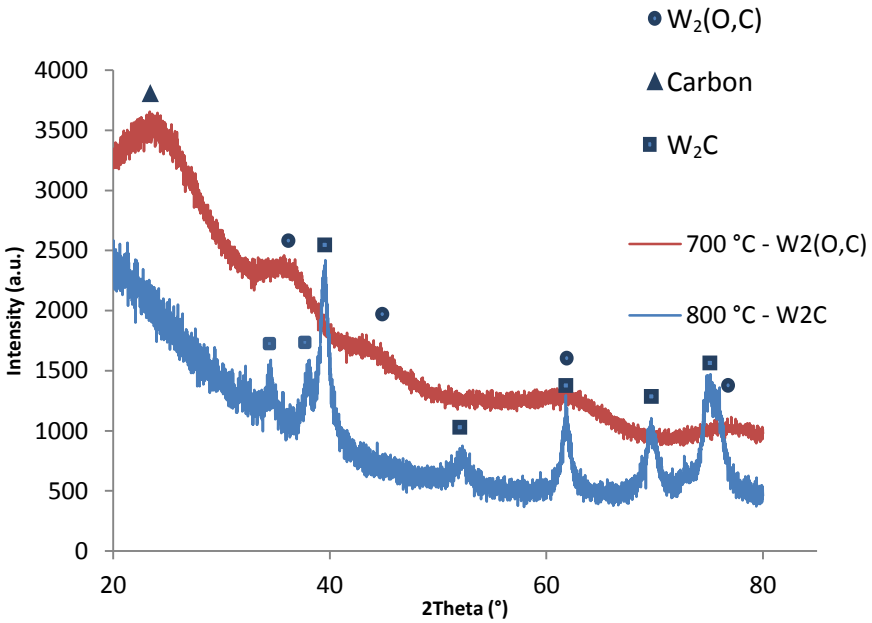

Figure 4.13: X-ray diffractogram of tungsten loaded N-doped carbon spheres treated at 700 and 800 °C.

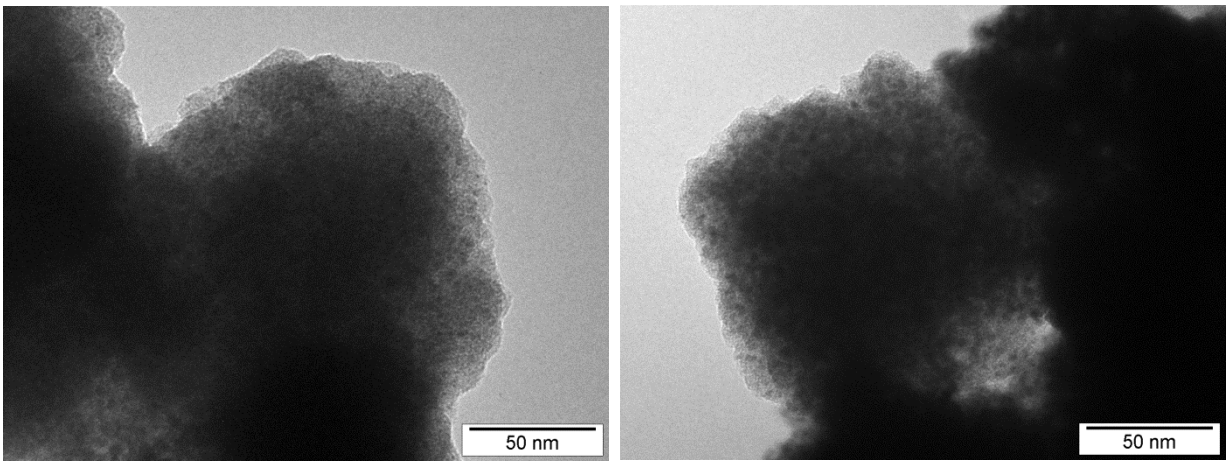

Figure 4.14: TEM micrograph of W-loaded nitrogen-doped carbon spheres, reduced at 800 °C in 80 % H_2/Ar

Despite the high temperature the carbon spheres maintained their shape and structure. The W_2C particles can be identified as small dark spots. They are well dispersed and have a size of approx. 4-5 nm. This shows that the nitrogen doping can maintain the particle distribution also at high synthesis temperatures.

In Figure 4.12 the TEM pictures suggest that the material treated at 700 °C still possesses an ordered mesoporous structure which cannot be found in the material treated at 800 °C in Figure 4.14. Therefore SAXS measurements were made to prove this hypothesis.

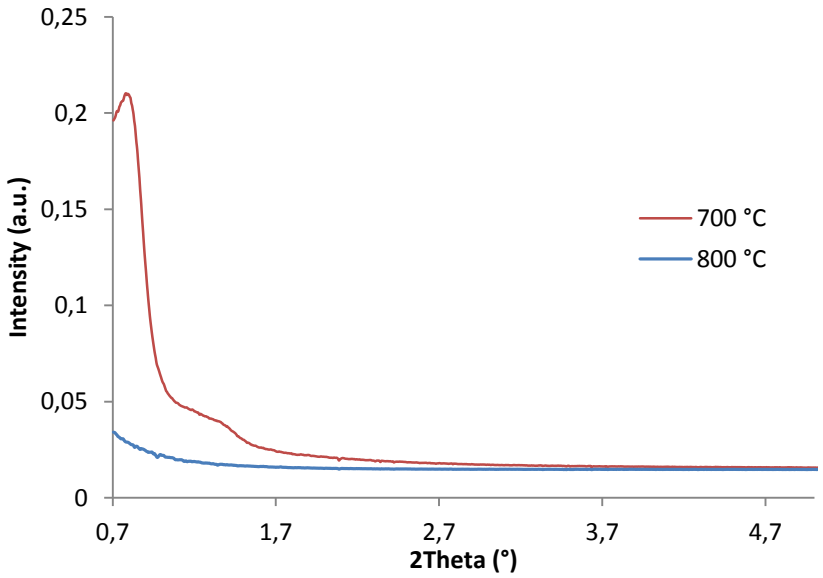

Figure 4.15 SAXS measurements of tungsten loaded N-doped polymer spheres treated at 700 °C and 800 °C, Calculated reflections for cubic phase (solid) and hexagonal phase (dashed)

If the mesostructured material possesses a hexagonal or a cubic phase cannot be determined definitely, because the scattering intensities are very low, which is due to the ratio between the pore radius and pore wall. In further experiments it may be investigated, if the mesostructure can be retained despite the carbide formation.

4.5 Tungsten carbide synthesis: Transition metal assisted synthesis

One disadvantage of the direct carbidization method is the high reaction temperature of 800 °C which causes a substantial material loss during the heating and growth of the carbide particles. Therefore other synthesis methods were investigated. It is known from literature that the addition of iron can facilitate the tungsten carbide formation.[63] This could enable the carbidization at lower temperature and without additional hydrogen. The reaction mechanism starts with the formation of $FeWO_4$ from the iron and the tungsten precursor. At higher temperatures $FeWO_4$ decomposes to Fe_3C and WC. This was also observed after the N-doped polymer spheres had been loaded with $K_4Fe(CN)_6$ and ammoniummetatungstate and heated to 700 °C under argon atmosphere. The corresponding X-ray diffractogram shows the formation of Fe_3C and WC, and after treating the material with acid the Fe_3C reflections

disappear, indicating the leaching of this compound. Only the WC phase and graphitic carbon are detected after the leaching. The reflections corresponding to graphitic carbon are surprising, as iron is a well-known graphitization catalyst.

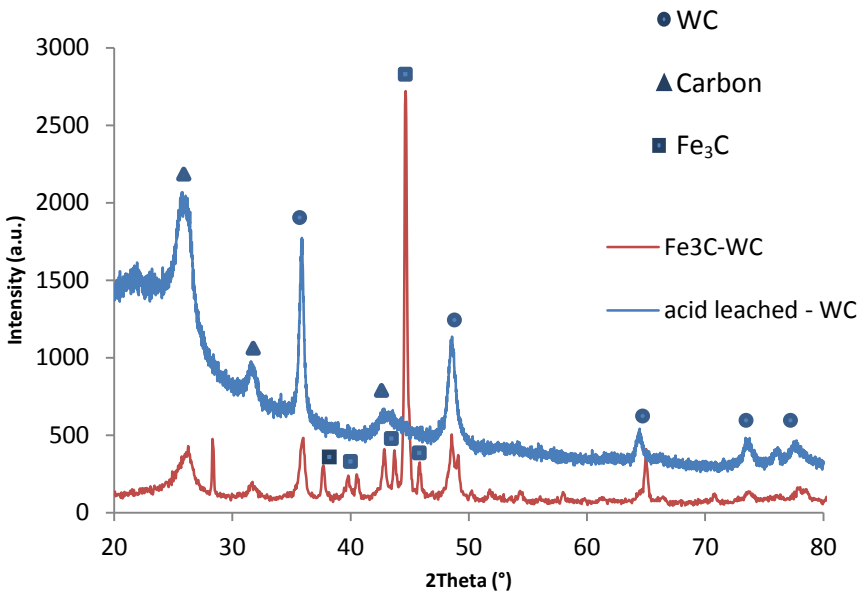

Figure 4.16: X-ray diffractogram of tungsten loaded N-doped carbon spheres: iron assisted synthesis before and after acid leaching

A remarkable difference compared to the previous synthesis method is that the formed tungsten carbide phase is WC, in contrast to the W_2C which is formed under the hydrogenating conditions without iron. This fact confirms the hypothesis of two different carbidization mechanisms, where the WC is derived from decomposition of $FeWO_4$ while W_2C is formed by stepwise reduction of WO_3 passing several, partially reduced intermediates like $W_2(O,C)$ before the final W_2C phase is reached.

$$WO_3 \longrightarrow WO_{3-x} \longrightarrow WO_xC_y \longrightarrow W_2C$$

The material was studied with TEM (Figure 4.17). The micrographs show two different kinds of particles which differ in size. The smaller particles are 10-20 nm in size and the bigger ones have sizes of 100 nm and more. One should also note the textural change of some of the carbon spheres. The visible, ordered mesoporous structure is lost, and replaced by an amorphous appearance. This is especially observed when bigger particles are formed in the carbon ball, implying that in these spots a great amount of Fe_3C is formed. There are two possible explanations for this structural change: The presence of a high iron loading in consequence of the big particles can induce more pronounced graphitization of the carbon support, causing the change of the mesostructure. Alternatively, the Fe_3C particle may consume such a high amount of carbon from the surrounding support material during its carbide formation that the carbon loss from the support leads to degradations of the mesostructure.

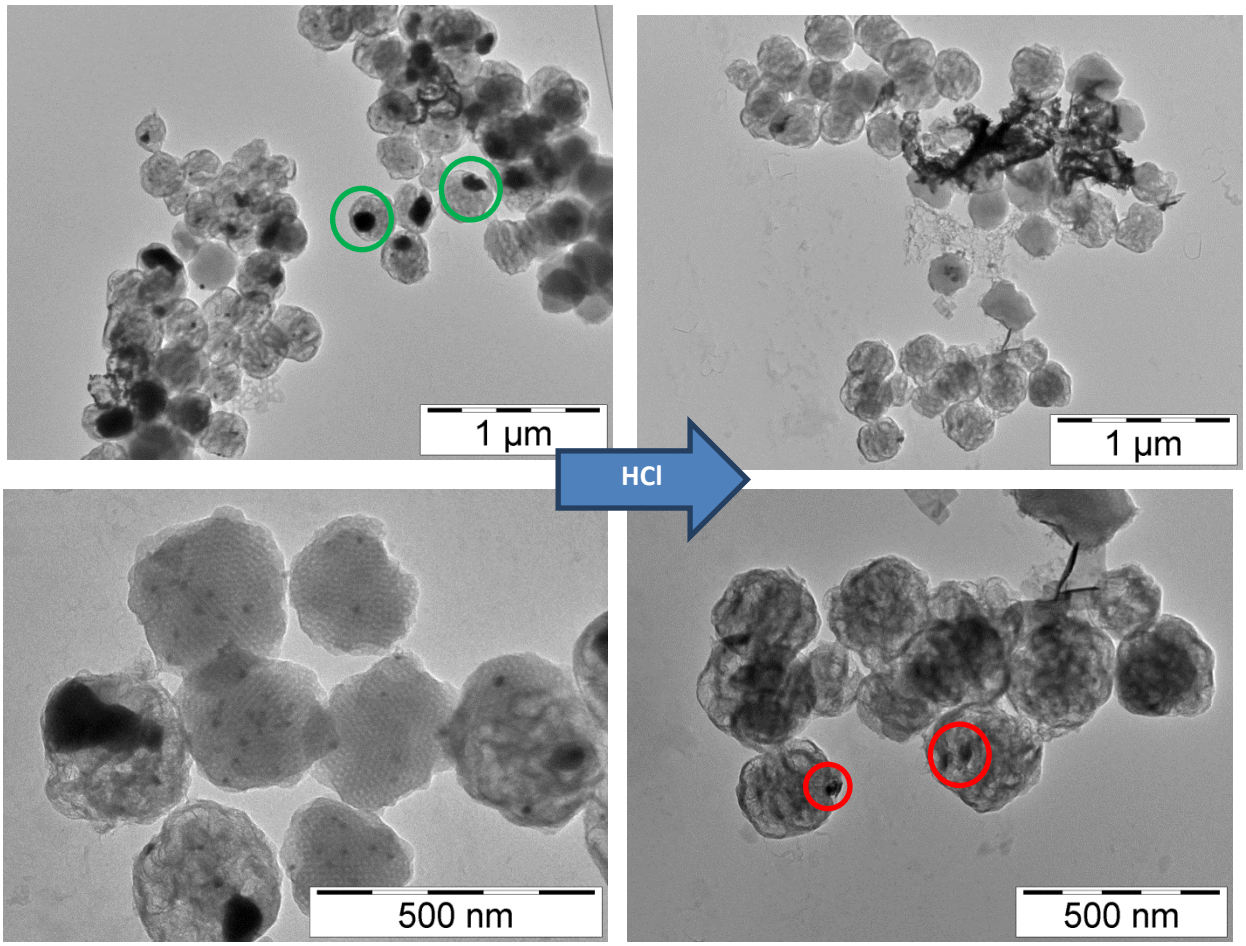

Figure 4.17: Mixed Fe_3C/WC on N-doped carbon spheres and the same sample without Fe_3C after acid treatment. Synthesis under pure argon atmosphere

After acid treatment, the big particles (green circle) cannot be found anymore in the micrographs, illustrating the leaching of the Fe_3C species. The vast majority is the remaining WC particles with a size of approx. 20 - 50 nm, but also single bigger particles of several 100 nm can still be found. The smaller particles that were present before the leaching could not be found afterwards. Additionally the distribution of the WC particles is quite inhomogeneous (red circles). It can be assumed that the Fe_3C and the WC form particles very close to each other, even mixed particles may form, since both carbide species are derived from the previously formed $FeWO_4$. This makes a good distribution very challenging as the Fe_3C particles can grow very large. One may thus conclude that the iron assisted carbidization is not the method of choice for this nanostructured support, as the distribution of the particles is not granted and the textural change of the carbon spheres is not uniform (some spheres are altered and others retain their characteristic texture).

Nevertheless, facilitating the carbide formation with a transition metal is an approach which seemed to merit further studies. The next step was thus the investigation of cobalt as assisting compound for the carbidization. Cobalt was chosen because it has similar chemical properties like iron and is also capable of forming the analogous $CoWO_4$ intermediate. The

XRD measurement identified WC as main phase but also other carbide phases like W_2C were detected, whereas the cobalt is present as the CoO phase. TEM micrographs show, besides some smaller particles with sizes of 10 – 20 nm, also big agglomerations of up to 100 nm. The transition metal allowed also in this case the carbide formation at lower temperature and without hydrogen. Unfortunately again the particle distribution is not satisfactory. The experiment was repeated under reductive atmosphere and with previous carbonization. This results are shown later in this chapter.

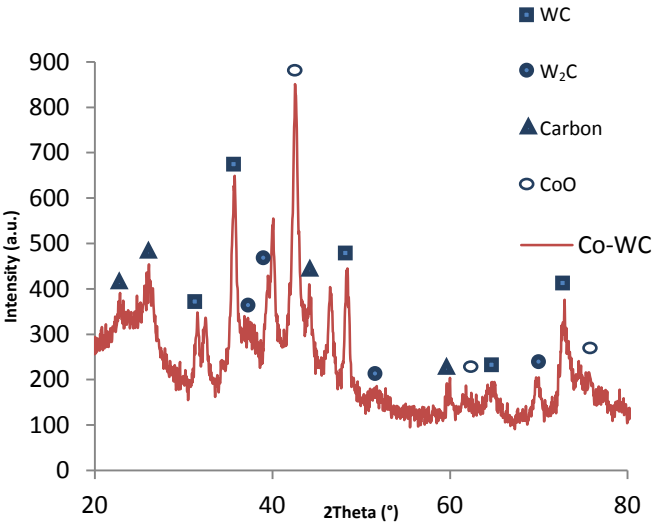

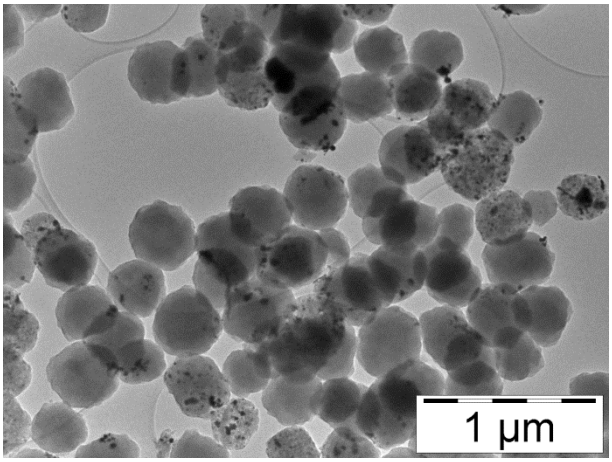

Figures 4.18 and 4.19: XRD pattern and TEM micrograph of cobalt mediated WC synthesis under pure argon atmosphere

The methods described so far need stoichiometric amounts of transition metals to facilitate the carbidization by formation of an intermediate tungstate. However, transition metals can also work via a different mechanism. It is found in literature that small amounts of nickel can facilitate the carbide formation under hydrogen atmosphere.[64] As a result the reaction temperature can be lowered. To study this reaction system in more detail, activated carbon was used at first as support material. Incipient wetness impregnation was performed with a mixed ammoniummetatungstate, nickel nitrate solution, where the nickel content was adjusted to 3-5 wt% (some deviations were observed due to loss of support). The impregnated catalysts were then heated to 700 °C once under an argon atmosphere and once under a 50% H_2/Ar atmosphere and subsequently analyzed with XRD (Figure 4.20).

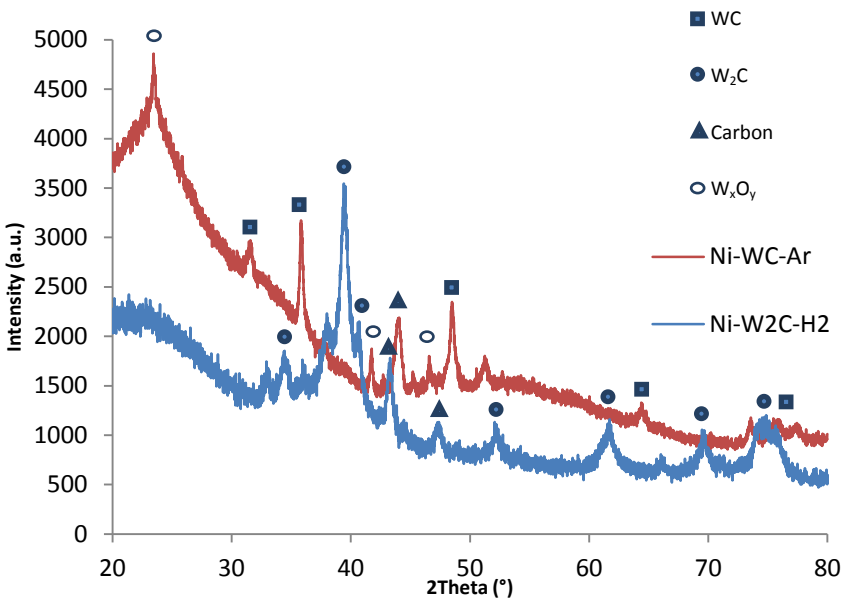

Figure 4.20: XRD pattern of tungsten carbides produced by nickel mediated synthesis on activated carbon. Comparison of pure argon atmosphere with mixed H_2/Ar atmosphere.

The XRD pattern shows that under argon atmosphere the mainly formed phase is WC. It seems that also nickel is capable of facilitating the carbidization process. Additionally tungsten oxide phases were detected. The incomplete conversion to the carbide can be explained by the low amount of nickel present in the sample, in contrast to the previous experiments, where stoichiometric amounts of transition metals had been added. The formation of WC is nevertheless higher than the present nickel concentration would suggest. Probably there exists a reaction mechanism for the nickel mediated carbidization that does not need stoichiometric metal amounts. This would differentiate it from the iron and cobalt mediated reactions. However, to prove this hypothesis, more detailed investigations would have been necessary that could not be conducted in the framework of this thesis.

In contrast, the X-ray diffractogram of the sample treated under mixed H_2/Ar flows shows W_2C as most prominent phase. The appearance of W_2C confirms again that under these reductive conditions the first discussed carbide formation pathway is taking place, which includes simultaneously the stepwise reduction of WO_3 and the carbidization. The addition of nickel seems to facilitate this reaction pathway, because nickel is a good hydrogenation catalyst and increases the availability of hydrogen at the surface of the material. This could lead to easier reduction of tungsten oxides so that full conversion to the carbide is achieved. No reflections in the diffractogram could be assigned to nickel-containing species, probably due to the low concentration or highly defective structures in combination with the tungsten, which would not give rise to pronounced reflections. The reductively treated material was investigated with TEM and the micrographs showed well dispersed particles between 5 and 20 nm. This material was further subjected to a reaction with TOP (same conditions like pure nickel containing materials) so that the incorporated nickel may be converted to nickel phosphide. This would yield a mixed Ni_2P – W_2C material, which could have interesting

catalytic properties, as a synergistic effect for catalytic reactions was reported in literature between W_2C and platinum group metals.[65] Since Ni_2P has a similar electronic structure as platinum group metals, a combination with W_2C might also be beneficial for catalytic activity. After reaction with TOP, the XRD measurement could not detect the Ni_2P phase, which is not surprising as the metallic nickel was neither detected, probably due to the low concentration However, it is likely that the phosphide was formed under those conditions. Therefore the material was examined with STEM measurements, where element mapping measurements were possible (Figure 4.21).

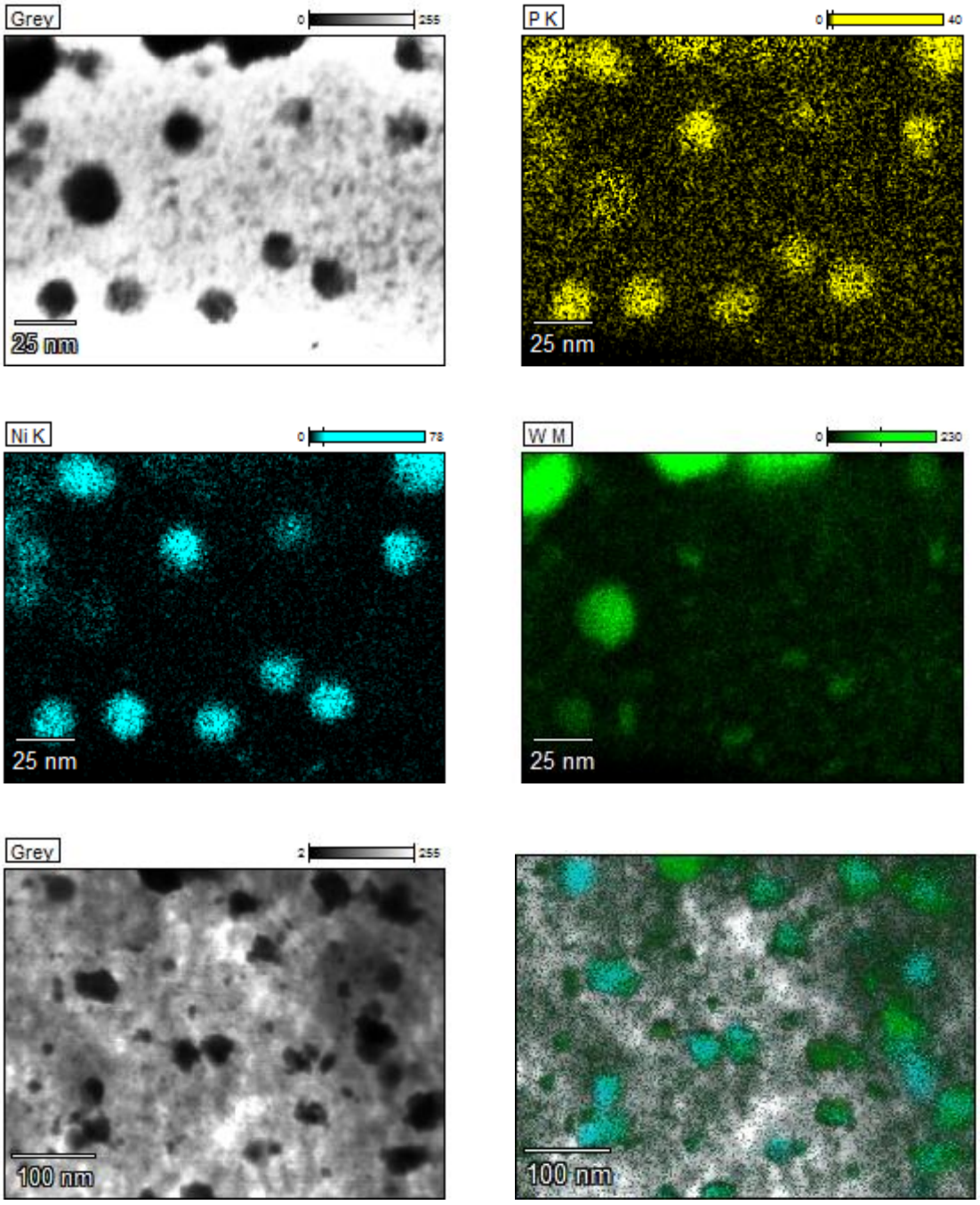

Figure 4.21: STEM micrographs and element mapping of mixed Ni_2P/W_2C on activated carbon, phosphorus (yellow), nickel (blue), tungsten (green)

The element mapping illustrates that the majority of the particles consists of pure W_2C, which is expected, because the tungsten loading was much higher. However, a significant number of particles contains a W_2C and a nickel part that are in direct contact with each other, considering the green (tungsten) and blue (nickel) coloring in the element mapping pictures. Even if the Ni_2P phase cannot be detected in XRD measurements, the areas with the highest phosphorous concentration are nearly identical with the areas of high nickel concentration, a distinct hint that a nickel phosphide phase has formed. Therefore it is assumed, the nickel in the material is present as Ni_2P. To obtain a lower concentration of the bigger particles, probably the tungsten loading has to be lowered, as in this material the tungsten loading is 30 wt.%. This experiment shows that a synthesis of mixed Ni_2P – W_2C particles is possible. This type of material could deliver insights in possible synergistic interactions between the two compounds for catalytic applications.

It was shown that small amount of nickel can enable the carbidization at 700 °C and reductive atmosphere. This method was also used with the nitrogen-doped carbon spheres as support material. The nitrogen-doped polymer spheres were loaded at the same time with ammoniummetatungstate and nickel nitrate by wetting impregnation. In contrast to the previous experiments the polymer spheres were not centrifuged after impregnation, but the liquid was evaporated. Otherwise the nickel cations would not stay on the polymer structure due to the repulsive interactions with the positively charged amino groups. Then the dried and loaded polymer spheres were heated firstly to 600 °C under a pure argon atmosphere to carbonize the polymers. Afterwards they were further heated under a mixed H_2/Ar atmosphere to 700 °C. After the reductive treatment and considering the weight loss of the support the calculated nickel content was 3%. The XRD pattern shows, besides the reflections attributed to metallic nickel particles, also reflections that can be attributed to carbide species, but also to metallic tungsten. The origin of the metallic tungsten can be either explained by it being an intermediate in the carbide formation or by reductive decomposition of the initially formed carbide. Which of these hypotheses is correct could not be clarified in the framework of this thesis, this would require a series of additional experiments under various atmospheres, temperatures and reaction times.

The TEM micrographs (Figure 4.22) shows that the majority of the particles formed single, well dispersed particles with sizes between 5 and 10 nm. However, also single bigger particles with the size of around 30 nm are found. Combining this fact with the information from the XRD, it is likely that these particles are containing non stoichiometric carbides, the metallic tungsten and nickel at the same time.

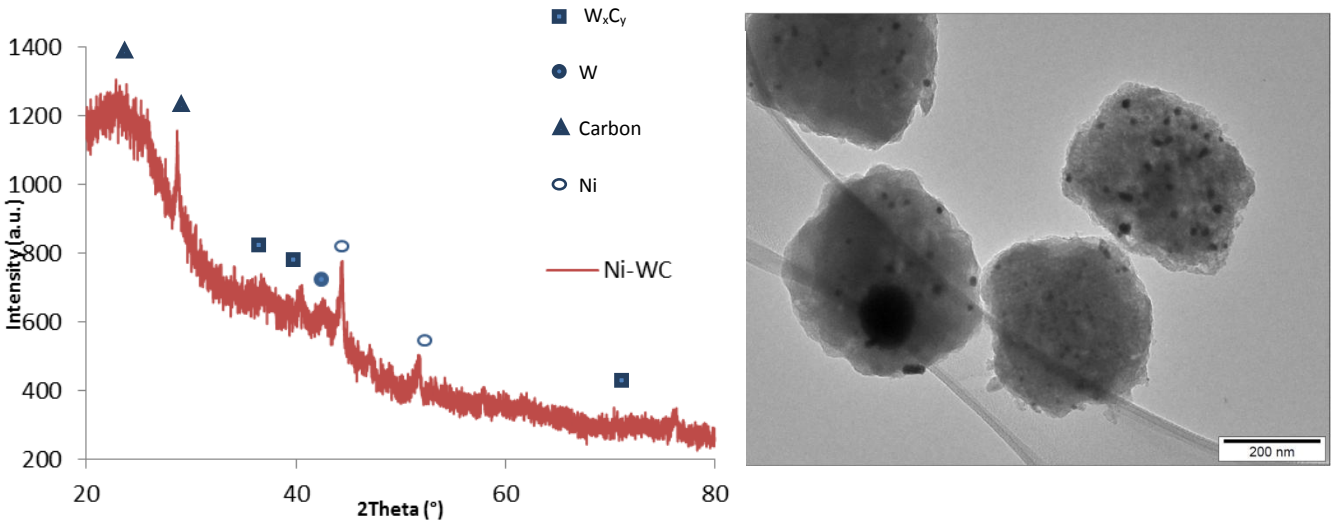

Figure 4.22: XRD pattern and TEM micrograph of nickel mediated WC synthesis on N-doped carbon spheres under reductive atmosphere

Finally it was tested if low amounts of cobalt could also facilitate the carbidization under reductive conditions. Therefore the N-doped polymer spheres were loaded with ammoniummetatungstate and $K_3Co(CN)_6$ at the same time. In this case the polymer spheres were centrifuged again, because the anionic cobalt species should interact with the cationic amino groups in the polymer, ensuring a good distribution in the polymer. Then the same carbonization and reductive protocol was applied as for the nickel doped polymers. The cobalt content was calculated to be 3 % for the reduced material. The X-ray diffractogram indicates that again W_2C was formed. In the range of 40-45 ° two very strong additional reflections appeared. The reflection at 43 ° may be attributed to the Co_2C phase as well as the smaller one at 45 ° (PDF Number 50-1371). The bigger reflection at 41 ° can be probably attributed to CoO, even if one peak alone cannot allow certain assignment of the peak (PDF Number 43-1004). The other reflections of CoO are superposed by the more intensive signals of the carbide. It can be concluded that the addition of cobalt enables the W_2C formation at 700 °C. Also cobalt is an active hydrogenation catalyst and probably works in a similar way as nickel. However, the TEM micrographs (Figure 4.23) indicate that there are similar problems as in the experiments conducted under argon atmosphere. Besides some smaller, well dispersed particles, very big agglomerations are found that also seem to have destroyed the neighboring carbon spheres.

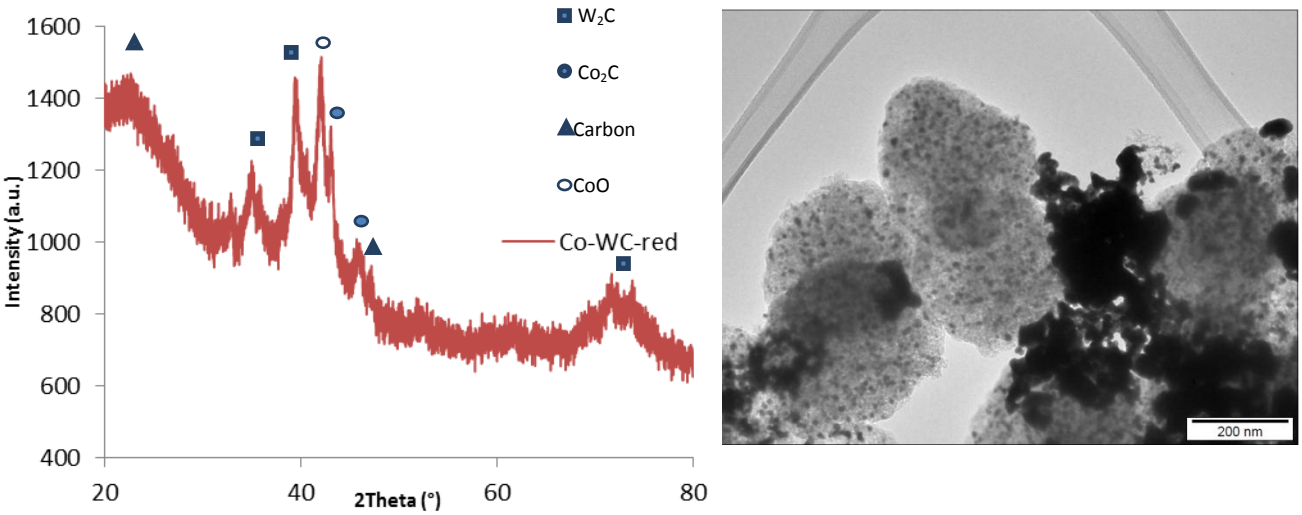

Figure 4.22: XRD pattern and TEM micrograph of cobalt mediated WC synthesis on N-doped carbon spheres under reductive atmosphere

From the experiments one may conclude that the metal mediated reactions are more challenging for the nitrogen-doped polymer than for conventional activated carbon. The cobalt mediated pathway produces the W_2C phases, however, very big particles and agglomerations are found. In contrast, in the nickel containing material small, well dispersed particles are formed, but the nature of the resulting phase is not clear, yet. Considering all the available facts and data it seems likely that changing the reaction conditions for the nickel containing material may result in the desired alteration of the phase composition towards the W_2C phase. Nevertheless this needs a more detailed investigation and variation of the reaction conditions, which could not be completed in the framework of this thesis. Recapitulating all the different carbidization protocolls it seems that so far only the direct carbidization without any transition metal at 800 °C can deliver the material with the desired characteristics. Nevertheless, in particular the nickel-mediated reactions have still optimization potential so that this pathway should be further explored.

5. Conclusion and Outlook

In this work different synthesis methods were used and compared that allow the formation of nanostructured Ni_2P particles. As a first step Ni_2P was synthesized on SiO_2 and activated carbon by the phosphite impregnation method. To gain a better control over the particle size and the distribution, alternative support materials should be studied. For this purpose hollow polymer shells containing free carboxylic acid groups were created by a soft-templating synthesis method and further used as support material. After treatment at elevated temperatures these polymer shells could be converted into carbon shells. It was also investigated, if loading the polymer shells, followed by carbonization, or previous carbonization, followed by loading with nickel/nickel phosphide, would give different results. The polymer and the carbon shells, respectively, were each loaded with nickel phosphide by impregnation and direct phosphidation. For impregnation, a nickel phosphite solution was used. The impregnated material was treated at 500 °C under a 10% H_2/Ar atmosphere to yield Ni_2P. In contrast, the direct phosphidation method consisted of two steps namely the deposition of metallic nickel particles and afterwards their conversion to Ni_2P. For loading the HPS with metallic nickel, a wetting impregnation was used, followed by a reduction at 500 °C. The deposition of nickel on HCS required a high temperature synthesis under inert atmosphere. Afterwards the metallic nickel was converted to Ni_2P with trioctylphosphane in a liquid phase reaction at 300 °C. It could be shown that direct phosphidation of metallic nickel particles would lead to smaller and better dispersed Ni_2P particles compared with the classical impregnation method. Comparing HPS and HCS for the direct phosphidation method, it became clear that that using polymer shells as support would yield smaller particles with a narrower size distribution (4.9 ± 1.5 vs. 6.7± 2.3 nm). TEM micrographs of the different materials are given in Figure 6.1.

Additionally this material has mesoporous properties and a BET surface area of 439 m^2/g (for the 10% loaded material). Good distribution and small particle size can only be obtained until a Ni_2P loading of approx. 10%. Loadings exceeding this value will cause the formation of additional single big particles of approx. 40 nm because there is not enough area on the shells to disperse higher Ni_2P amounts. However, the HPS derived material treated under direct phosphidation conditions yielded the Ni_2P particles with the smallest size and the best distribution. Also the BET surface area was higher compared to the HCS derived material. A final advantage is that the metallic nickel is loaded onto the HPS with wetting impregnation, whereas for the HCS a high temperature procedure under inert atmosphere is required.

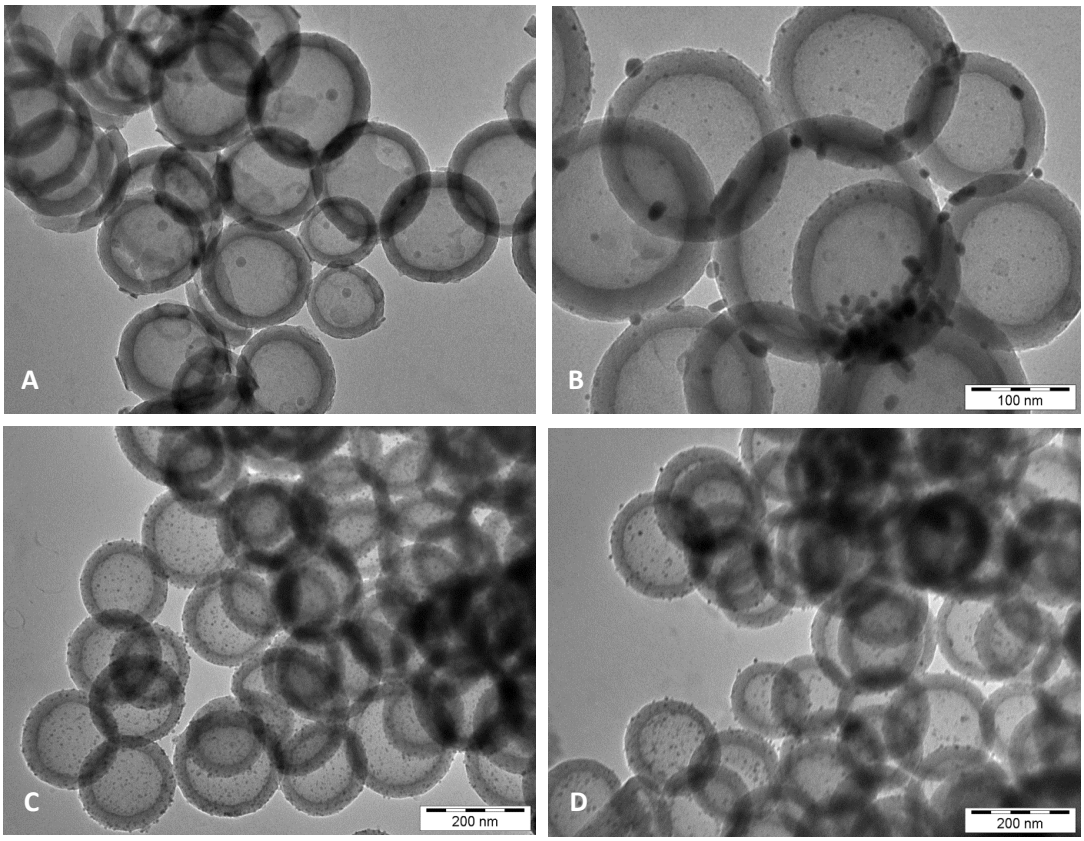

Figure 6.1: TEM micrographs of (A) Ni_2P/HPS – impr., (B) Ni_2P/HCS – impr., (C) Ni_2P/HPS – direct phosphidation, (D) Ni_2P/HCS – direct phosphidation

To use this material in a catalytic reaction it has to be activated at 500 °C under argon atmosphere to remove the remaining TOP from the pore system. An additional activation at lower temperatures and under reductive atmosphere has to be performed to remove the oxide surface species. The exact activation protocols should still be further developed to find the lowest temperature that allows the removal of the pore blocking species and the surface oxides.

The next step in the study of these materials should be an extensive catalytic testing for the HDO reaction. At first reactions with model substrates such as phenol, guajacol or furans, should be performed. These experiments will give information about the optimal reaction conditions and catalyst stability. Therefore different temperatures, pressures and solvents have to be tested, and it needs to be evaluated how changing these factors affects product yield and selectivity. When the best reaction conditions are established and the catalysts exhibited sufficient stability, the tests can be extended to compound mixtures and real bio-oil. Only these tests will show if a use of the Ni_2P material will also be feasible on bigger scale.

The second goal of this work was the synthesis of nanostructured tungsten carbide. The hollow polymer shells were impregnated with ammoniummetatungstate and then treated at high temperatures and under reductive atmosphere. The formation of W_2C could be proven, but the TEM micrographs revealed that the resulting particles are not well dispersed; also the particle size was too big. This was attributed to the anionic nature of the carboxylic acid groups, which were not able to disperse the metatungstate anions. An additional problem was the instability of the carbon shells under the synthesis conditions; partial degradation was observed. To ensure a better distribution of the carbide particles and prevent the decomposition of the support, a different support material was chosen. Nitrogen doped polymer spheres with a more rigid structure containing ordered mesopores were created. The amino groups present in the material are cationic under acidic conditions and should allow a better distribution of the tungsten species. The polymer spheres were loaded with the tungsten precursor, and the analysis following treatment at 700 °C under a mixed H_2/Ar did not reveal indications of degradation. Also the formation of small particles could be detected by TEM. However, according to XRD measurements these particles consisted of $W_2(O,C)$ which is only an intermediate of the carbide formation. Therefore, prior to the carbide formation a carbonization of the polymer spheres was conducted at 600 °C under argon atmosphere. The reductive procedure was subsequently repeated at 800 °C yielding slightly bigger particles. The XRD investigation suggested that the formed phase is W_2C.

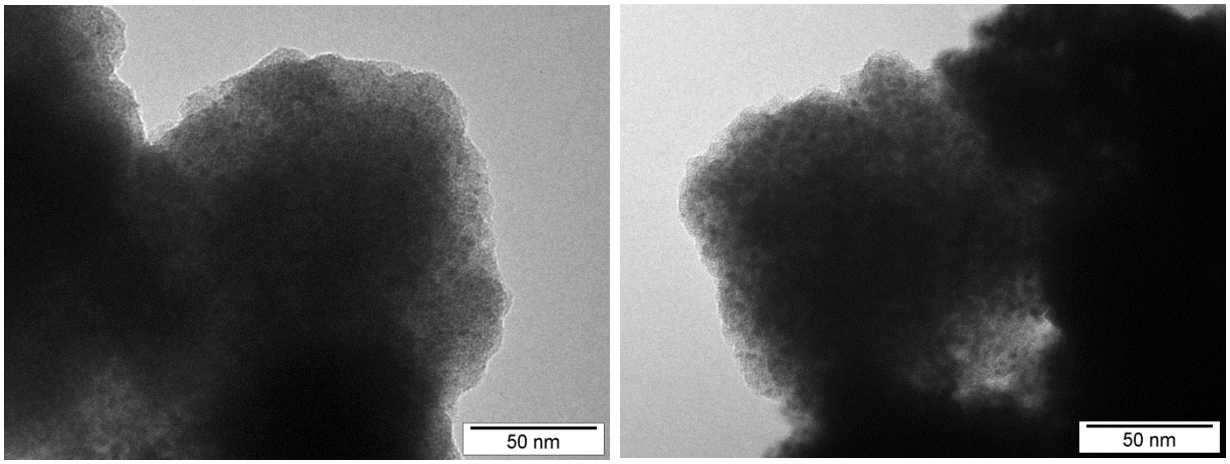

Figure 6.2: TEM micrograph of W-loaded nitrogen-doped carbon spheres, reduced at 800 °C in 80 % H_2/Ar

The carbide particles have a size of 3-4 nm and are well dispersed. The change of the support material has served its purpose and allowed the formation of small, well dispersed W_2C particles without decomposition of the support material. It should be noted that a central step in all the carbide formation protocols is the carbonization at 600 °C under argon atmosphere. Without this step the carbide formation will not take place to this extent and also the material loss will by higher.

Still, the synthesis temperatures for the carbide are comparatively high with 800 °C, which causes also relatively high loss of material during the synthesis. Due to this reason further

strategies, which were supposed to allow the carbide formation at lower temperatures, were investigated. By addition of transition metals like iron or cobalt the carbidization could be completed at 700 °C and under inert atmosphere (only argon). These metals can mediate the carbidization by formation of intermediate species like $FeWO_4$ and $CoWO_4$. At higher temperatures they decompose and form WC and the carbide of the other transition metal at the same. It should also be highlighted that under these conditions WC is the formed phase, in contrast to the synthesis under reductive conditions, where W_2C, is formed, due to different formation mechanisms. The resulting WC particles are quite polydisperse and have sizes of up to 100 nm; they are also not well dispersed over the support. Even if the transition metals allow the formation of WC at lower temperatures and non-reductive atmosphere the desired nanostructuring could not be achieved on this substrate.

Transition metals can also facilitate the carbidization under reductive conditions. This process was investigated by impregnating the tungsten loaded support material with small amounts (1-3 wt. %) of nickel. This reaction type was firstly studied using activated carbon as support. Under a mixed H_2/Ar atmosphere the formation of W_2C could be observed already at 700 °C, when the tungsten loaded activated carbon was additionally impregnated with nickel. Nickel is a well-known hydrogenation catalyst and increases the availability of hydrogen on the surface, which might facilitate the reduction of the oxidic tungsten species to the carbide.

When a pure argon atmosphere (also at 700 °C) is used, the mainly formed phase is WC and not W_2C. This illustrates how the carbidization mechanism, depends on the used reaction atmosphere. Changing between reductive and inert reaction conditions could thus be a possible control mechanism to adjust the nature of the carbide phase.

The reaction was also studied on the N-doped polymer/carbon support under reductive atmosphere. The polymer support was impregnated with nickel and the tungsten precursor. The sample was carbonized at 600 °C and reduced at 700 °C. The XRD pattern suggested the formation of a non-defined carbide phase, besides metallic tungsten and nickel phases. The TEM micrographs prove that the majority of the particles consists of small dispersed ones with a size between 5 and 10 nm but also single big particles up to 50 nm can be found.

It was tested if also cobalt could induce the formation of W_2C under reductive conditions. Therefore an anionic cobalt precursor was loaded onto the N-doped polymer spheres, together with ammoniummetatungstate. It was assumed that the anionic cobalt precursor ($K_3Co(CN)_6$) would allow a better distribution in the support material compared to the cationic nickel. This should enable a more homogeneous particle formation. The sample underwent the same high temperature treatment conditions as the nickel containing material. Also here the formation of W_2C was confirmed by the X-ray diffractograms. It seems that cobalt works also as hydrogenation catalyst, in a similar way as nickel, and can also facilitate the carbidization under inert and reductive conditions. However, the TEM micrographs showed that very big particles and agglomerations formed beside the small particles.

The metal assisted carbide formation on the N-doped carbon spheres showed that with nickel well dispersed, small particles are formed, but the carbide phase is a non-stoichiometric compound and also some metallic tungsten is formed. For the cobalt mediated reaction W_2C was the main carbide phase, but the particles showed partially severe agglomeration. Nevertheless, specifically the nickel assisted synthesis seems to have the potential to create the desired nanostructured materials, if the phase formation can be better controlled. It is likely that changing the reaction conditions for the nickel containing material may result in the desired change of the phase towards the W_2C. Future experiments should therefore consider investigating and varying the reaction conditions systematically to obtain more information about the formation of the phases.

The carbidization protocols that are reported in this work can serve as a starting point for more detailed investigations of this reaction. Especially the transition metal assisted carbidization should be investigated in detail. The reaction conditions (gas composition, heating rates and reaction time) should be optimized to produce the particles with the smallest possible size. Also the reaction mechanism can still be studied as it was shown that also small amounts of nickel could induce the WC formation, although it is commonly accepted that at least stoichiometric amounts of transition metal are needed for this task. Especially the formed intermediate products have to be analyzed. With more knowledge about this type of reaction it should then be possible in future to obtain nanostructured carbides in the desired phase which are produced under non-reductive conditions. The nickel mediated carbidization provides also an additional perspective, namely the synthesis of combined Ni_2P – W_2C materials. The general possibility to create such a material on conventional activated carbon could already be shown in this work. The next step should be the extension of the fabrication of this combined material to nanostructured supports, because this special material may have great potential for catalytic application as HDO catalyst. It will allow investigating possible synergistic interactions between the carbide and the phosphide phase.

The gained insights and reaction mechanisms can be also used for the synthesis of molybdenum carbide containing materials. Mo_2C has very similar characteristics compared with its tungsten analogue. Thus similar reaction conditions can be applied for its synthesis. Furthermore it is also active in the HDO reaction and should also be studied for this reaction especially in comparison with the tungsten carbides.

Nevertheless, the material that was already obtained in this work, by temperature treatment at 800 °C and without any metal mediation, has still to be investigated for its catalytic activity. Also here detailed catalytic tests for HDO reactions are the next step for the W_2C on N-doped carbon spheres. At first tests with the same model compounds like for Ni_2P (guajacol, phenol) are required, followed by the optimization of reaction conditions. If the results are satisfactory the catalyst can also be tested for bio-oils. Besides the application as HDO

catalyst the W_2C on N-doped carbon has also another possible applications. Tungsten carbides are already used in literature as fuel cell catalysts, due to their platinum like reactivity.[65] Also this W_2C material should be tested as fuel cell catalyst, since the particle size is low and the distribution is good. Furthermore the N-doped carbon spheres have a mesoporous structure which may be beneficial for any kind of diffusion and transport phenomena. Additionally it was already shown in the literature that fuel cell catalysts supported on nanostructured carbon shells or spheres exhibit high activity and cycle stability.[66]

6. Experimental

6.1 Chemicals

Silica gel was acquired from Sigma-Aldrich as TLC high purity grade (5−25 µm particle diameter; 0.75 cm^3/g total pore volume; product number 288519) and activated Carbon was purchased from Cabot Norit (particle diameter d50: 30 µm, 1400 m^2/g BET surface area; product name Norit CA1). Both materials were dried by heating in an oil vacuum prior to use. All other chemicals were acquired by Sigma-Aldrich, Fluka or Acros and used as received.

6.2 Synthesis

6.2.1 Hollow polymer shells and hollow carbon shells

The hollow polymer shells were produced as reported by G.H. Wang et al. [67] 0.185 g of 2,4-dihydroxybenzoic acid and 0.070 g hexamethylenetetramine were dissolved in 60 mL deionized water. Followed by addition of 20 mL of an aqueous solution, containing 0.044 g Pluronic® P123 and 0.073 g sodium oleate, was added under slow stirring. After stirring for 10 min, the mixed solution was transferred into a Teflon-lined stainless-steel autoclave of 120 mL capacity, sealed, heated to 160 °C with a heating rate of 1 °C min^{-1} and maintained at that temperature for 2 h. Afterwards, the autoclave was allowed to cool to room temperature. The red-brown solid products were collected by centrifugation at 16500 min^{-1} for 10 min (Sigma 3K30, 12156-H, angle rotor 8 × 50 mL), washed three times with deionized water, and finally dried at 50 °C under vacuum for 8 h.

To obtain the hollow carbon shells, the hollow polymer shells underwent pyrolysis under argon atmosphere under the following conditions: the sample was heated from room temperature to 400 °C with a rate of 2 °C min^{-1} and kept at this temperature for 3 h, and then heated to 500 °C with a rate of 1 °C min^{-1} and kept at this temperature for 2 h. Afterwards, the sample was allowed to cool to room temperature in flowing argon.

6.2.2 Synthesis of Ni-HCS – Ion exchange

Typically 400 mg of hollow polymer shells were dispersed by ultrasonication in 20 mL aqueous 5 % NH_3 solution where the desired amount of $Ni(NO_3)_2*6H_2O$ had been dissolved prior to that. Then the dispersion was heated to 50 °C and stirred with a magnetic stirring bar for 5 h, followed by centrifugation at 16500 min^{-1} for 10 min and washing two times with deionized water and drying at 50 °C under vacuum for 8 h.

To obtain the nickel loaded hollow carbon shells, the hollow polymer shells underwent pyrolysis in 10 % H_2 in argon atmosphere at following conditions: the sample was heated to 400 °C with a rate of 2 °C min^{-1} and held at this temperature for 3 h, and then heated to 500 °C with a rate of 1 °C min^{-1} and held at this temperature for 2 h. Afterwards the sample

was allowed to cool to room temperature followed by passivation for 1 h in a gas stream of 1% O_2 in N_2. The metal loaded particles were characterized with XRD and TEM.

6.2.3 Synthesis of Ni on Support – Direct

An evacuated and argon flushed Schlenk-tube was loaded with 1.50 g triphenylphosphane and a magnetic stirring bar and heated to 150 ° C. Under counter current argon flow 150-200 mg of the desired support material (activated carbon or hollow carbon shells) were added and dispersed by stirring. The dispersion was then heated to 200 °C whereupon the desired amount of $Ni(acac)_2$ and 1.5 mL oleylamine were added under counter current argon flow. The reaction solution was stirred for 2 h at this temperature and then cooled to room temperature. Finally ethanol was added to settle the dispersed particles. This solution was then centrifuged at 16500 min^{-1} for 10 min, washed two times with ethanol, and then dried at 50 °C under vacuum for 8 h. The metal loaded particles were characterized with XRD and TEM.

6.2.4 Phosphidation

An evacuated and argon flushed Schlenk-tube was loaded with 3 mL dioctylether and heated to 290 °C. In a separate glass vial 150-200 mg of the nickel loaded supports from chapters 6.2.2 or 6.2.3 are dispersed in 3 mL trioctylphosphane. This dispersion was rapidly injected into the hot dioctylether and then heated to 300 °C holding this temperature for 6 h before cooling to room temperature. The particles were settled by addition of ethanol and the dispersion is then centrifuged at 16500 min^{-1} for 10 min washed two times with ethanol and then dried at 50 °C under vacuum for 8 h. The particles were characterized with XRD to confirm the conversion to Ni_2P and TEM.

6.2.5 Synthesis of Ni_2P – Incipient wetness impregnation

A solution of $Ni(H_2PO_3)_2$ was prepared by ultrasonication of 0.37 g (0.004 mol) $Ni(OH)_2$ and 0.66 g (0.008 mol) H_3PO_3 in 2 mL H_2O for 2 h yielding a clear green solution. The desired amount of this solution was diluted with deionized water to the incipient volume for the particular support. Then the support was impregnated and dried at 50 °C under vacuum for 12 h.

Table 7.1 Incipient volumes of different supports

Support	**Incipient volume [µL] for 100 mg support**
SiO_2	150
Activated carbon	200
Hollow polymer shells	75
Hollow carbon shells	120

The dried impregnated support was then transferred to a tubular furnace and heated to 400 °C with a heating rate of 2 °C min^{-1} under a gas flow of 200 mL min^{-1} 10% H_2 in Ar. This temperature was kept for 3 h followed by heating to 500 °C with a heating rate of 1 °C min^{-1} and the latter temperature was kept for 2 h. After that the sample was cooled to room temperature and passivated in a flow of 1 % O_2 in N_2.

6.2.6 Synthesis of N-doped polymer spheres

0.654 g aminophenol and 0.420 g hexamethylenetetramine were dissolved in 75 mL deionized water in a 100 - mL flask. When the compounds were completely dissolved, 5 mL of a solution containing 0.125 g/mL Pluronic® F127 was added and the solution was heated to 80 °C and stirred with a magnetic stirring bar for 24 h. Hereafter the system was cooled down to room temperature and centrifuged at 16500 min^{-1} for 8 min. The obtained brown solid product was washed two times with deionized water and dried at 50 °C in vacuum for 12 h.

6.2.7 Synthesis of WC/W_2C – gas phase carbidization/ metal assisted carbidization (inert atmosphere)

The desired amount of ammoniummetatungstate (12 mg or 36 mg) was dissolved in 10 mL of 1 M HCl. If iron or cobalt should also be introduced into the polymer spheres the corresponding compound ($K_4Fe(CN)_6$ (weight ratio W:Fe=1:5) or $K_3Co(CN)_6$ (weight ratio W:Co=2:1) respectively) was also dissolved. 180 mg of N-doped polymer spheres were dispersed in this solution by ultrasonication. Then the dispersion was heated to 50 °C and stirred with a magnetic stirring bar for 24 h. Hereafter the system was cooled down to room temperature and centrifuged at 16500 min^{-1} for 8 min washed two times with deionized water and dried at 50 °C in vacuum for 12 h.

Several protocols for carbonization were realized:

The gas flow rates were adjusted to 150 mL/min for all experiments. After completing the synthesis, all materials were passivated in 1 % O_2/N_2 for 1 h.

- Only tungsten loaded: Heating from 25 °C to 700 °C in 10 h and holding this temperature for 3 h under 50% H_2/Ar or 10 % Ethane, 40 % argon and 50 % H_2.

- Only tungsten loaded - Pre-carbonisation: Heating from 25 °C to 600 °C in 10 h and holding at this temperature for 3 h under pure argon. After cooling down: heating up again from 25 °C to 450 °C in 30 min then to 800 °C in 5 h and holding at this temperature for 3 h under a pure H_2 atmosphere (125 mL/min H_2, 300 mg carbonized sample). The carbonization is essential that the material can withstand the reductive conditions. The carbidization time at 800 °C may vary with the amount of sample in

the oven and the hydrogen flow. It should be remarked that a bigger sample amount can need more time for the thermal treatment.

- Fe or Co & tungsten loaded – inert atmosphere: Heating from 25 °C to 450 °C in 2 h then to 700 °C in 4 h and holding at this temperature for 3 h under pure Ar.

6.2.8 Metal assisted carbidization (Ni or Co under reductive atmosphere):

The desired amount of ammoniummetatungstate (12 mg or 36 mg) was dissolved in 10 mL of 1 M HCl. 8 mg of $Ni(NO_3)_2*6H_2O$ or 10 mg of $K_3Co(CN)_6$ were also dissolved. 180 mg of N-doped polymer spheres were dispersed in this solution by ultrasonication. Then the dispersion was heated to 50 °C and stirred with a magnetic stirring bar for 24 h. The cobalt containing material was separated by centrifugation, whereas the nickel loaded polymer was directly dried by evaporation of the water under reduced pressure. The dried polymer was then carbonized by heating from 25 °C to 600 °C in 10 h and this temperature was held for 3 h under pure Ar atmosphere. After cooling down the sample, it was heated up again from 25 °C to 450 °C in 30 min then to 700 °C in 4 h and held at this temperature for 1 h under an atmosphere of 50 % H_2/Ar.

6.2.9 Synthesis of W_2C and Mo_2C on activated carbon or HCS – direct carbidization

The desired amount of ammoniummetatungstate hydrate (W≤66.7%) or ammoniumheptamolybdate was dissolved in the incipient wetness volume of the chosen amount of activated carbon or HCS followed by impregnation of the carbon. The impregnated carbon was dried at 50 °C in vacuum for 8 h.

The dried sample was transferred into a quartz reactor inside a tubular resistance furnace. A stream of 100 mL min^{-1} H_2 and Ar (1:1) was passed through the reactor. The reaction temperature was increased to 450 °C in 30 min, followed by heating to 800 °C in 6 h where the temperature was held for 1 h. After that the sample was cooled down to room temperature and passivated in a stream of 1% O_2/N_2. For samples impregnated with ammoniumheptamolybdate the maximum temperature was 750 °C.

6.3 Characterization

6.3.1 Transmission electron microscopy (TEM)

TEM images were recorded on Hitachi HF7500 and Hitachi HF2000 microscopes. The solid sample was dispersed by ultrasonication in ethanol and dropped onto a copper/lacy carbon grid. After drying any loose material was removed by shaking the grid. The TEM measurements were performed at the MPI für Kohlenforschung in Mülheim by Dr. Guanghui Wang. The combined STEM and element mapping measurements were conducted at a Hitachi S-5500 ultra-high resolution cold field emission scanning electron microscope. The

instrument was operated at a maximum acceleration voltage of 30 kV. The samples were prepared on Lacey carbon films supported on a 400 mesh copper grid. The measurements were performed by Mr. Hans Bongard.

6.3.2 X-ray diffraction

Powder X-ray diffraction (XRD) was performed on a STOE Stadi P diffractometer operating in reflection mode (Bragg-Brentano geometry) with CuKα radiation, using a secondary graphite monochromator. Transmission XRD measurements were performed on a STOE Stadi P transmission X-ray diffractometer using $CuK\alpha_1$ radiation. The instrument is equipped with a primary monochromator and a linear position-selective detector. All measurements were performed in a glass capillary.

6.3.3 Sorption

The nitrogen sorption measurements were carried out on a Quantachrome NOVA 3000e instrument and on a Micrometrics ASAP 2010 instrument. Prior to analysis, the samples were activated under oil vacuum for at least 8 h at 200 °C. The measurements were performed at -195.80 °C using a static-volumetric method. The empty volume was determined with nitrogen. The used measurement parameters are pressure tolerance 0.1 Torr, equilibration time 60 seconds and equilibrium timeout 160 seconds. The Brunauer-Emmett-Teller specific surface area (BET s.a.) is determined using five data points between 0.1 and 0.25 relative pressure p/p_0.

6.3.4 Elemental analysis

The elemental analysis was carried out by “Mikroanalytisches Laboratorium Kolbe” who quantified the nickel content with AAS and the phosphorous content by a chromatographic analysis.

6.3.5 SAXS

The measurements were performed on an Anton Paar SAXSess instrument equipped with a Kratky-camera and measured with $CuK\alpha_1$ (1.54051 Å) radiation with line focus. The samples were prepared in 0.7 mm glass capillaries with a wall diameter of 0.1 mm. For data analysis the scattering curve of the unloaded HCS material was subtracted as underground from the loaded material. The measurements were performed by Dr. Wolfgang Schmidt.

7. Appendix

List of Figures

8. Abbreviations

AAS	Atomic absorption spectroscopy
Act. C	Activated Carbon
approx.	Approximately
°C	Degree Celsius
DDO	Direct deoxygenation
et al.	et alii
etc.	et cetera
EU	European union
FCC	Fluid catalytic cracking
Fig.	Figure
F-T	Fischer-Tropsch
g	Gram
h	hour
HCS	Hollow carbon shells
HDN	Hydrodenitrification
HDO	Hydrodeoxygenation
HDS	Hydrodesulfurization
HPS	Hollow polymer shells
HYD	Hydrogenation
kg	Kilogram
L	Liter
m	Meter
min	Minute
mL	Milliliter
mm	Millimeter
MJ	Megajoule
nm	Nanometer
ppm	Parts per million

Ref.	Reference
SAXS	Small angle X-ray scattering
TEM	Transmission electron microscopy
TOP	Trioctylphosphane
TMS	Transition metal sulfide
XRD	X-ray diffraction

9. References

[1] S. Solomon, G.-K. Plattner, R. Knutti, P. Friedlingstein, *Proc. Natl. Acad. Sci. USA* **2009**, *106*, 1704–1709.

[2] L. Chiari, A. Zecca, *Energ. Policy* **2011**, *39*, 5026–5034.

[3] B. für W. und Energie, *Energiedaten Ges. Aus.* **2014**.

[4] N. Armaroli, V. Balzani, *Angew. Chem. Int. Ed.* **2007**, *46*, 52–66.

[5] E. Gnansounou, *Bioresour. Technol.* **2010**, *101*, 4842–50.

[6] G. W. Huber, S. Iborra, A. Corma, *Chem. Rev.* **2006**, *106*, 4044–98.

[7] P. Kumar, D. M. Barrett, M. J. Delwiche, P. Stroeve, *Ind. Eng. Chem. Res.* **2009**, *48*, 3713–3729.

[8] S. N. Naik, V. V. Goud, P. K. Rout, A. K. Dalai, *Renew. Sustain. Energy Rev.* **2010**, *14*, 578–597.

[9] D. A. Ruddy, J. A. Schaidle, J. R. Ferrell III, J. Wang, L. Moens, J. E. Hensley, *Green Chem.* **2014**, *16*, 454–490.

[10] R. B. Levy, M. Boudart, *Science* **1973**, *181*, 547–549.

[11] Y. Shu, S. T. Oyama, *Carbon* **2005**, *43*, 1517–1532.

[12] S. T. Oyama, T. Gott, H. Zhao, Y.-K. Lee, *Catal. Today* **2009**, *143*, 94–107.

[13] European Commission, “Europe 2020 – Europe’s growth strategy,” DOI 10.1016/j.resconrec.2010.03.010can be found under http://ec.europa.eu/europe2020/index_en.htm, **2011**.

[14] S. P. S. Chundawat, G. T. Beckham, M. E. Himmel, B. E. Dale, *Annu. Rev. Chem. Biomol. Eng.* **2011**, *2*, 121–45.

[15] N. Meine, R. Rinaldi, F. Schüth, *ChemSusChem* **2012**, *5*, 1449–1454.

[16] R. J. Evans, T. A. Milne, *Energ. Fuel.* **1987**, *1*, 123–138.

[17] E. van Steen, M. Claeys, *Chem. Eng. Technol.* **2008**, *31*, 655–666.

[18] A. V. Bridgwater, *Biomass Bioenerg.* **2012**, *38*, 68–94.

[19] C. Branca, P. Giudicianni, C. Di Blasi, *Ind. Eng. Chem. Res.* **2003**, *42*, 3190–3202.

[20] P. Grange, E. Laurent, R. Maggi, A. Centeno, B. Delmon, *Catal. Today* **1996**, *29*, 297–301.

[21] R. J. M. Westerhof, N. J. M. Kuipers, S. R. A. Kersten, W. P. M. Van Swaaij, *Ind. Eng. Chem. Res.*, **2007**, 9238–9247.

[22] S. Czernik, A. V. Bridgwater, *Energ. Fuel.* **2004**, *18*, 590–598.

[23] J. C. Serrano-Ruiz, J. A. Dumesic, *Energy Environ. Sci.* **2011**, *4*, 83.

[24] A. C. Hansen, Q. Zhang, P. W. L. Lyne, *Bioresour. Technol.* **2005**, *96*, 277–285.

[25] G. W. Huber, A. Corma, *Angew. Chem.* **2007**, *119*, 7320–7338.

[26] A. G. Gayubo, A. T. Aguayo, A. Atutxa, B. Valle, J. Bilbao, *J. Chem. Technol. Biotechnol.* **2005**, *80*, 1244–1251.

[27] A. Corma, G. W. Huber, L. Sauvanaud, P. O'Connor, *J. Catal.* **2007**, *247*, 307–327.

[28] P. M. Mortensen, J. Grunwaldt, P. A. Jensen, K. G. Knudsen, A. D. Jensen, *Appl. Catal. A-Gen.* **2011**, *407*, 1–19.

[29] J. Lauritsen, *J. Catal.* **2001**, *197*, 1–5.

[30] M. Badawi, J.-F. Paul, E. Payen, Y. Romero, F. Richard, S. Brunet, a. Popov, E. Kondratieva, J.-P. Gilson, L. Mariey, *Oil Gas Sci. Technol. – Rev. d'IFP Energies Nouv.* **2013**, *68*, 829–840.

[31] E. Furimsky, *Catal. Today* **1999**, *52*, 381–495.

[32] V. N. Bui, D. Laurenti, P. Afanasiev, C. Geantet, *Appl. Catal. B-Environ.* **2011**, *101*, 239–245.

[33] A. Gutierrez, R. K. Kaila, M. L. Honkela, R. Slioor, A. O. I. Krause, *Catal. Today* **2009**, *147*, 239–246.

[34] T. Nimmanwudipong, R. C. Runnebaum, D. E. Block, B. C. Gates, *Energ. Fuel.* **2011**, *25*, 3417–3427.

[35] C. Newman, X. Zhou, B. Goundie, I. T. Ghampson, R. a. Pollock, Z. Ross, M. C. Wheeler, R. W. Meulenberg, R. N. Austin, B. G. Frederick, *Appl. Catal. A-Gen.* **2014**, *477*, 64–74.

[36] D. Gao, C. Schweitzer, H. T. Hwang, A. Varma, *Ind. Eng. Chem. Res.* **2014**, Article ASAP.

[37] M. Saidi, F. Samimi, D. Karimipourfard, T. Nimmanwudipong, B. C. Gates, M. R. Rahimpour, *Energy Environ. Sci.* **2014**, *7*, 103.

[38] R. B. Levy, M. Boudart, *Science* **1973**, *181*, 547–9.

[39] E. L. M. and J. C. Sauer, *J. Am. Chem. Soc.* **1974**, *11*, 3410–3415.

[40] S. Oyama, *J. Catal.* **2003**, *216*, 343–352.

[41] S. Ted Oyama, H. Zhao, H.-J. Freund, K. Asakura, R. Włodarczyk, M. Sierka, *J. Catal.* **2012**, *285*, 1–5.

[42] A. S. Kurlov, A. I. Gusev, *Inorg. Mater.* **2006**, *42*, 121–127.

[43] T. Xiao, A. Hanif, A. P. E. York, J. Sloan, M. L. H. Green, *Phys. Chem. Chem. Phys.* **2002**, *4*, 3522–3529.

[44] C. Liang, F. Tian, Z. Li, Z. Feng, *Chem. Mater.* **2003**, *15*, 4846–4853.

[45] R. W. Gosselink, D. R. Stellwagen, J. H. Bitter, *Angew. Chem.* **2013**, *125*, 5193–5196.

[46] A. L. Jongerius, R. W. Gosselink, J. Dijkstra, J. H. Bitter, P. C. a. Bruijnincx, B. M. Weckhuysen, *ChemCatChem* **2013**, *5*, 2964–2972.

[47] K. Xiong, W.-S. Lee, A. Bhan, J. G. Chen, *ChemSusChem* **2014**, *10027*, 1–5.

[48] H. Okamoto, *J. Phase Equilib.* **2000**, *21*, 210–210.

[49] Y. Yang, C. Ochoa-herna, A. De Pen, O. Shea, J. M. Coronado, D. P. Serrano, *ACS Catal.* **2012**, *2*, 592–598.

[50] Q. Guan, W. Li, M. Zhang, K. Tao, *J. Catal.* **2009**, *263*, 1–3.

[51] J. a. Cecilia, A. Infantes-Molina, E. Rodriguez-Castellon, A. Jimenez-Lopez, *J. Catal.* **2009**, *263*, 4–15.

[52] J. Park, B. Koo, K. Y. Yoon, Y. Hwang, M. Kang, J.-G. Park, T. Hyeon, *J. Am. Chem. Soc.* **2005**, *127*, 8433–40.

[53] R. Prins, M. E. Bussell, *Catal. Lett.* **2012**, *142*, 1413–1436.

[54] P. Bui, J. A. Cecilia, S. T. Oyama, A. Takagaki, A. Infantes-Molina, H. Zhao, D. Li, E. Rodriguez-Castellon, A. Jimenez Lopez, *J. Catal.* **2012**, *294*, 184–198.

[55] S.-K. Wu, P.-C. Lai, Y.-C. Lin, H.-P. Wan, H.-T. Lee, Y.-H. Chang, *ACS Sustain. Chem. Eng.* **2013**, *1*, 349–358.

[56] J. a. Cecilia, A. Infantes-Molina, E. Rodriguez-Castellon, A. Jimenez-Lopez, S. T. Oyama, *Appl. Catal. B-Environ.* **2013**, *136-137*, 140–149.

[57] Y. Yang, J. Chen, H. Shi, *Energ. Fuel.* **2013**, *27*, 3400.

[58] S. T. Oyama, X. Wang, Y.-K. Lee, W.-J. Chun, *J. Catal.* **2004**, *221*, 263–273.

[59] V. M. L. Whiffen, K. J. Smith, *Top. Catal.* **2012**, *55*, 981.

[60] H. Y. Zhao, D. Li, P. Bui, S. T. Oyama, *Appl. Catal. A-Gen.* **2011**, *391*, 305–310.

[61] J.-S. Moon, E.-G. Kim, Y.-K. Lee, *J. Catal.* **2014**, *311*, 144–152.

[62] X. Wang, *J. Catal.* **2002**, *208*, 321–331.

[63] Z. Yan, M. Cai, P. K. Shen, *Sci. Rep.* **2013**, *3*, 1646.

[64] Y.-B. Huang, M.-Y. Chen, L. Yan, Q.-X. Guo, Y. Fu, *ChemSusChem* **2014**, *7*, 1068–72.

[65] R. Ganesan, J. S. Lee, *Angew. Chem. Int. Ed.* **2005**, *44*, 6557–6560.

[66] C. Galeano, J. C. Meier, V. Peinecke, H. Bongard, I. Katsounaros, A. A. Topalov, A. Lu, K. J. J. Mayrhofer, F. Schüth, *J. Am. Chem. Soc.* **2012**, *134*, 20457–20465.

[67] G. Wang, J. Hilgert, F. H. Richter, F. Wang, H. Bongard, B. Spliethoff, C. Weidenthaler, F. Schüth, *Nat. Mater.* **2014**, *13*, 297-300.

Eidesstattliche Erklärung

AFFIDAVIT

Ich erkläre an Eides statt, dass ich die vorliegende Arbeit selbstständig verfasst, andere als die angegebenen Quellen/Hilfsmittel nicht benutzt, und die den benutzten Quellen wörtlich und inhaltlich entnommenen Stellen als solche kenntlich gemacht habe. Das in TUGRAZonline hochgeladene Textdokument ist mit der vorliegenden Masterarbeit identisch.

I declare that I have authored this thesis independently, that I have not used other than the declared sources/resources, and that I have explicitly indicated all material which has been quoted either literally or by content from the sources used. The text document uploaded to TUGRAZonline is identical to the present master's thesis.

Datum / Date

Unterschrift / Signature